

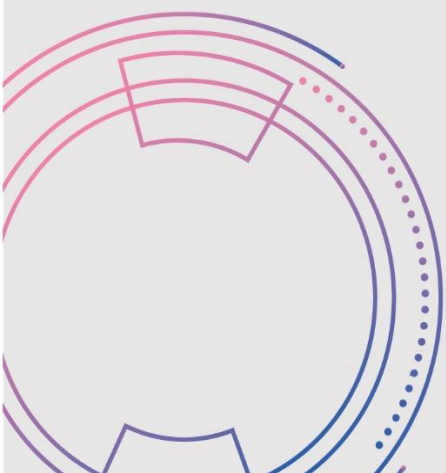


**Firat University
Journal of Experimental
and Computational
Engineering**

Volume: 1

Issues: 2

Year: 2022



Owner

On Behalf of Firat University

Rector

Prof. Dr. Fahrettin GÖKTAŞ

Editor-in-Chief

Prof. Dr. Mehmet YILMAZ, Firat University, Turkey

Vice Editor-in-Chief

Prof. Dr. Ebru AKPINAR, Firat University, Turkey

Prof. Dr. Ragıp İNCE, Firat University, Turkey

Prof. Dr. Levent TAŞÇI, Firat University, Turkey

Prof. Dr. Yakup DEMİR, Firat University, Turkey

Prof. Dr. Mete Onur KAMAN, Firat University, Turkey

Assoc. Prof. Dr. Erkut YALÇIN, Firat University, Turkey

Editorial Advisory Board

Prof. Dr. Abdulkadir Cüneyt AYDIN, Atatürk University, Turkey

Prof. Dr. Abdussamet ARSLAN, Gazi University, Turkey

Prof. Dr. Ahmet ŞAŞMAZ, Firat University, Turkey

Prof. Dr. Arif GÜLTEN, Firat University, Turkey

Prof. Dr. Baha Vural KÖK, Firat University, Turkey

Prof. Dr. Bilal ALATAŞ, Firat University, Turkey

Prof. Dr. Erhan AKIN, Firat University, Turkey

Prof. Dr. Erkan KÖSE, Nuh Naci Yazgan University, Turkey

Prof. Dr. Filiz KAR, Firat University, Turkey

Prof. Dr. Hasan SOFUOĞLU, Karadeniz Technical University, Turkey

Prof. Dr. İhsan DAĞTEKİN, Firat University, Turkey

Prof. Dr. İsmail Hakkı ALTAŞ, Karadeniz Technical University, Turkey

Prof. Dr. Kazım TÜRK, İnönü University, Turkey

Prof. Dr. M. Şaban TANYILDIZI, Firat University, Turkey

Prof. Dr. Mehmet KARAKÖSE, Firat University, Turkey

Prof. Dr. Mehtap MURATOĞLU, Firat University, Turkey

Prof. Dr. Nevin ÇELİK, Firat University, Turkey

Prof. Dr. Oğuz GÜNGÖR, Ankara University, Turkey

Prof. Dr. Oğuz YAKUT, Firat University, Turkey

Prof. Dr. Özge Kaya HANAY, Firat University, Turkey

Prof. Dr. Paki TURGUT, İnönü University, Turkey

Prof. Dr. Selçuk ÇEBİ, Yıldız Technical University, Turkey

Prof. Dr. Taner ALATAŞ, Firat University, Turkey

Prof. Dr. Yusuf AYVAZ, Yıldız Technical University, Turkey

Assoc. Prof. Dr. Fatih ÖZYURT, Firat University, Turkey

Editorial Board

Prof. Dr. Mehmet YILMAZ (Editor-in-Chief)	Civil Engineering
Prof. Dr. Ebru AKPINAR (Vice Editor-in-Chief)	Mechanical Engineering
Prof. Dr. Ragıp İNCE (Vice Editor-in-Chief)	Civil Engineering
Prof. Dr. Levent TAŞÇI (Vice Editor-in-Chief)	Civil Engineering
Prof. Dr. Yakup DEMİR (Vice Editor-in-Chief)	Electrical-Electronics Engineering
Prof. Dr. Mete Onur KAMAN (Vice Editor-in-Chief)	Mechanical Engineering
Assoc. Prof. Dr. Erkut YALÇIN (Vice Editor-in-Chief)	Civil Engineering
Prof. Dr. Abdullah Hilmi LAV	Civil Engineering
Prof. Dr. Ali TOPAL	Civil Engineering
Prof. Dr. Ali YAZICI	Software Engineering
Prof. Dr. Arif GAYDAROV	Chemical Engineering
Prof. Dr. Ayşe Vildan BEŞE	Chemical Engineering
Prof. Dr. Bilge Hilal CADIRCI EFELİ	Bioengineering
Prof. Dr. Ertan EVİN	Mechanical Engineering
Prof. Dr. Evren Meltem TOYGAR	Mechanical Engineering
Prof. Dr. Gülşad Uslu ŞENEL	Environmental Engineering
Prof. Dr. Kadir TURAN	Mechanical Engineering
Prof. Dr. H. Soner ALTUNDOĞAN	Bioengineering
Prof. Dr. Mehmet Deniz TURAN	Metallurgy and Materials Engineering
Prof. Dr. Mehmet YETMEZ	Mechanical Engineering
Prof. Dr. Murat ELİBOL	Bioengineering
Prof. Dr. Mustafa YANALAK	Geodesy and Photog. Engineering
Prof. Dr. Nicola TARQUE	Civil Engineering
Prof. Dr. Nuno MENDES	Mechanical Engineering
Prof. Dr. Rashid NADİROV	Chemical
Prof. Dr. Serdar Ethem HAMAMCI	Electrical-Electronics Engineering
Prof. Dr. Vizureanu PETRICA	Material Processing Technologies
Prof. Dr. VLadimir RYBAKOV	Mathematics and Computer Science
Assoc. Prof. Dr. Alvaro Garcia HERNANDEZ	Civil Engineering
Assoc. Prof. Dr. Baigenzhenov OMİRSERİK	Metallurgical Engineering
Assoc. Prof. Dr. Ebru DURAL	Civil Engineering
Assoc. Prof. Dr. Edip AVŞAR	Environmental Engineering
Assoc. Prof. Dr. Ersin Yener YAZICI	Mining Engineering
Assoc. Prof. Dr. Fatih ÇETİŞLİ	Civil Engineering
Assoc. Prof. Dr. Jülide ÖNER	Civil Engineering
Assoc. Prof. Dr. Marcin SAJDAK	Environmental Engineering and Energy
Assoc. Prof. Dr. Ömer GÖKKUŞ	Environmental Engineering
Assoc. Prof. Dr. Serdar ÇARBAŞ	Civil Engineering
Assoc. Prof. Dr. Tacettin GEÇKİL	Civil Engineering
Assoc. Prof. Dr. Erkut YALÇIN	Civil Engineering
Assist. Prof. Dr. Alvaro Aracena CAIPA	Chemical Engineering
Assist. Prof. Dr. Bahadır YILMAZ	Civil Engineering
Assist. Prof. Dr. Durmuş YARIMPABUÇ	Mathematics
Assist. Prof. Dr. Serap KOÇ	Mechanical Engineering
Assist. Prof. Dr. Ömer Saltuk BÖLÜKBAŞI	Metallurgy and Materials Engineering
Assist. Prof. Dr. Özlem AYDIN	Fod Engineering
Dr. Amilton Barbosa Botelho JUNİOR	Chemical Engineering
Dr. Norman TORO	Metallurgical Engineering
Res. Assist. Dr. Dragana BOZIC	Mining and Metallurgy Institute
Res. Assist. Dr. Jelena MİLOJKOVIĆ	Mineral Raw Materials Tech. Institute
Res. Assist. Dr. Serkan ERDEM	Civil Engineering
Res. Assist. Dr. Ulaş Baran BALOĞLU	Computer Engineering
Res. Assist. Shoeleh ASSEMI	Material Engineering
Lecturer Abdullah Gökhan TUĞAN (Language Editor)	English Language Teaching
Mustafa Gani GENÇER (Language Editor)	English Language Teaching
Res. Assist. Dr. Özge Erdoğan YAMAÇ (Pub. Coordinators)	Civil Engineering
Res. Assist. Beyza Furtana YALÇIN (Secretariat)	Civil Engineering

Composition

Hakan YURDAKUL

Correspondence Address

Firat University Faculty of Engineering Journal of Experimental and Computational Engineering Publishing Coordinatorship
23119 Elazığ/TÜRKİYE

E-mail: fujece@firat.edu.tr

Web page: <http://fujece.firat.edu.tr/>

Firat University Journal of Experimental and Computational Engineering a peer-reviewed journal.

CONTENTS

Surface characterization of commercial chitosan with SEM and BET techniques (Research Article) SEM ve BET teknikleri ile ticari kitosanın yüzey karakterizasyonu (Araştırma Makalesi)	
Fatih KAYA, Şeyda TAŞAR, Ahmet ÖZER	43
Modeling the limiting performance of resistive superconductor fault current limiters for 2G HTS tape (Research Article) Rezistif süperiletken arıza akımı sınırlayıcıların sınırlandırma performansının 2G HTS şerit için modellenmesi (Araştırma Makalesi)	
Buğra YILMAZ, Muhsin Tunay GENÇOĞLU	49
Characterization of polyurethane produced by polyol synthesized from corn oil (Research Article) Mısır yağından sentezlenen poliolden üretilen poliüretanın karakterizasyonu (Araştırma Makalesi)	
Ercan AYDOĞMUŞ, Fethi KAMIŞLI	60
Production and characterization of chitosan-based polymer particles with the precipitation collection method (Research Article) Çöktürme toplama metodu ile kitosan esaslı polimerik partikül üretimi ve karakterizasyonu (Araştırma Makalesi)	
Hülya DEMİRTAŞ, Şeyda TAŞAR, Fatih KAYA, Ahmet ÖZER	68
A novel design for concrete culverts absorbing explosive energy from homemade explosives (Research Article) Ev yapımı patlayıcılardan oluşan patlayıcı enerjisini sönmüleyen beton büzler için yeni bir tasarım (Araştırma Makalesi)	
Sedat SAVAŞ, Dursun BAKIR, Muharrem BAŞPINAR, Mehmet ÜLKER	80



Surface characterization of commercial chitosan with SEM and BET techniques

SEM ve BET teknikleri ile ticari kitosanın yüzey karakterizasyonu

Fatih KAYA^{1*} , Şeyda TAŞAR² , Ahmet ÖZER³ 

^{1,2,3} Department of Chemical Engineering, Faculty of Engineering, Firat University, Elazig, Turkey.

¹fatihkaya@firat.edu.tr, ²sydtasar@firat.edu.tr, ³aozer@firat.edu.tr

Received: 20.01.2022
Accepted: 09.05.2022

Revision: 22.04.2022

doi: 10.5505/fujece.2022.09797
Research Article

Abstract

Chitosan, a natural polymer, has recently been the focus of attention of researchers due to its superior properties such as biocompatible, biodegradable, renewable, and low toxicity. Especially in the fields of chemistry and health sciences, its use as a wound dressing material, adsorbent, resin, drug carrier system, and food packaging is being researched. This study, it is aimed to contribute to the areas where chitosan is used as adsorbent, resin, and wound dressing material by making surface characterization. According to the data obtained from the study, it was determined that chitosan was a non-porous polymer with a membranous surface. In addition, it was determined that there may be calcium particles as a surface impurity on the surface of commercial chitosan samples.

Keywords: Chitosan, SEM and BET techniques, Morphological analysis.

Özet

Doğal bir polimer olan kitosan biyoyoumlu, biyobozunur, yenilenebilir ve düşük toksisite gibi üstün özellikleri sebebiyle son zamanlarda araştırmacıların ilgi odağı olmuştur. Özellikle kimya ve sağlık bilimleri gibi alanlarda yara örtü malzemesi, adsorbent, reçine, ilaç salınımı ve gıda ambalajı olarak çalışılmaktadır. Bu çalışmada kitosanın yüzey karakterizasyonu yapılarak onun adsorbent, reçine ve yara örtü malzemesi olarak kullanıldığı alanlara katkıda bulunulması amaçlanmıştır. Çalışmadan elde edilen verilere göre kitosanın gözeneksiz ve zarımsı yüzeye sahip bir polimer olduğu tespit edilmiştir. Ayrıca, ticari kitosan örneklerinin yüzeyinde bir yüzey safsızlığı olarak kalsiyum parçacıklarının da olabileceği saptanmıştır.

Anahtar kelimeler: Kitosan, SEM ve BET teknikleri, Morfolojik analiz.

1. Introduction

Chitin and chitosan polymers are natural amino polysaccharides. These polymers have a unique structure with their multidimensional/directional properties and their application areas are quite wide. They have many positive features such as low toxicity, ecological safety, antimicrobial activity, low immunogenicity, excellent biocompatibility, and biodegradability [1]. In addition to these features, their renewable, low-cost and chemically functional nature have increased the interest in chitin and chitosan, making them the subject of research in many fields such as chemistry, environment, food packing/coating, biotechnology, and medicine.

Chitin is the second most abundant polymer in nature after cellulose. Cellulose is obtained from the cell walls of plants, and chitin is obtained from fungus or the shells of insects or crustaceans. Cellulose and chitin are macromolecules that maintain the structural integrity of plants and animals, respectively. In this respect, it is possible to say that cellulose and chitin are structurally related polysaccharides. In addition, there is a great similarity between chitin and cellulose in terms of molecular structure. Instead of hydroxyl groups (-OH) at the C2 position of cellulose, chitin has acetamide groups (CH₃-(C=O)-NH-), while chitosan has primary amine (-NH₂) groups. It is possible to name chitin and chitosan as renewable polymers, biopolymers, or natural polymers. But chitin is a homopolymer. It consists of N-Acetyl-D-Glucosamine

*Corresponding author

monomers as the kit shows in Figure 1. Chitosan, on the other hand, is a copolymer consisting of N-Acetyl-D-Glucosamine and D-Glucosamine monomers [1-3].

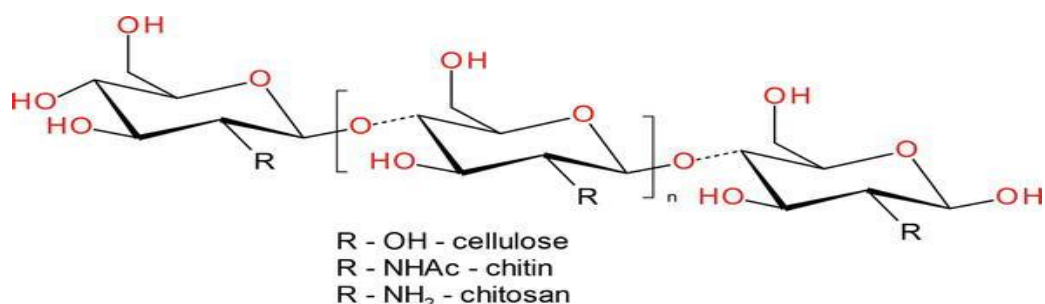


Figure 1. The molecular similarity of chitin, chitosan, and cellulose [4]

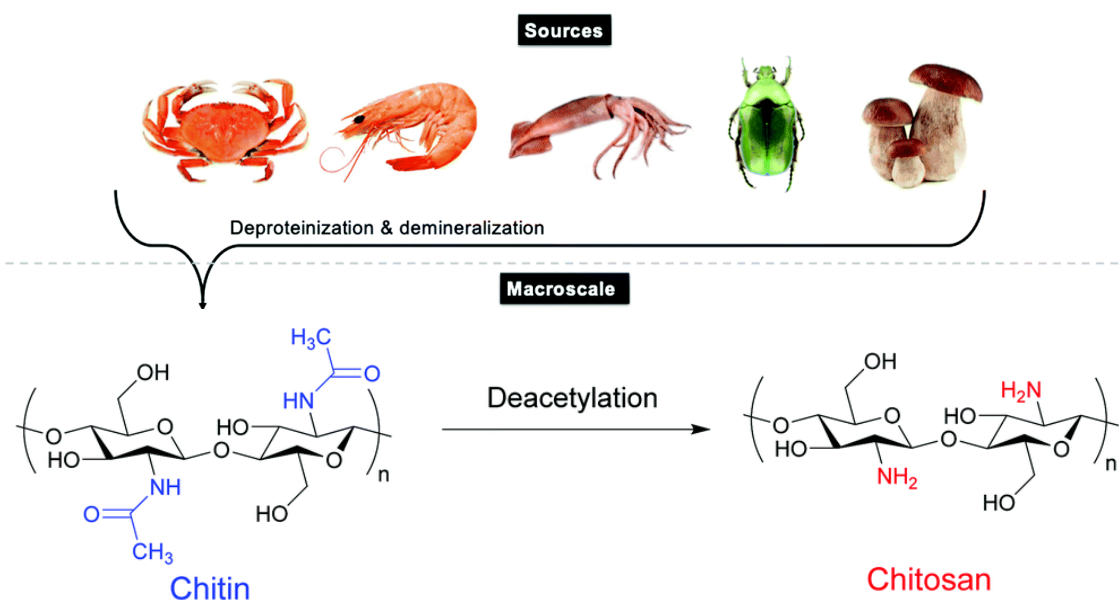


Figure 2. Chemical structures of chitin and chitosan via deacetylation [5]

Chitin is produced industrially from mushrooms or the shells of shellfish such as shrimp. Chitosan is the primary derivative produced by the alkaline deacetylation of chitin (Figure 2). The production of chitosan from shellfish waste occurs in three basic stages. These basic steps can be listed as de-mineralization (DM), deproteinization (DP), and de-acetylation (DA). At the end of the DM and DP processes, chitin is produced from waste shells. With the DA process, which is the last step, the conversion of chitin into chitosan is achieved [3, 6].

There are three important physicochemical properties used to describe the chitosan macromolecule. These are the degree of deacetylation (DD), molecular weight (Mw), and solubility. The most obvious difference between chitin and chitosan is that their solubility properties are different. Because chitin has strong intramolecular and intermolecular hydrogen bonds, it is insoluble in conventional solvents, including organic solvents and mineral acids. The low solubility of chitin may limit its use. Therefore, there is a need for more easily soluble derivatives such as chitosan. Acetic acid, lactic acid, oxalic acid, formic acid, and pyruvic acid can be used as solvents for chitosan. The most commonly used solvent for chitosan is dilute acetic acid solution. The dissolution of chitosan occurs through the protonation of amine groups. The percentage of primary amine groups in the polymer chain of chitosan relative to the acetamide groups is defined as the degree of deacetylation. The de-acetylation degree and molecular weight of chitosan can vary depending on the reaction conditions in the chitosan production process [1, 3, 7, 8].

Since chitosan is biocompatible, biodegradable, and has low toxicity, it has been the focus of interest in medical studies. In this context, chitosan has started to be used in the development of wound dressing materials, gene therapy, and the development of controlled drug release systems [7, 9, 10]. In addition, the fact that chitosan is the second most abundant polymer in nature and has active chemical groups such as amine and hydroxyl in its chemical structure has made it the focus of attention in the field of chemistry. It is widely used especially as an adsorbent and resin. It is possible to come across many studies in the literature in which chitosan or modified chitosan derivatives are used as sorbents [2, 11]. A sorption process is a surface event that takes place through the pores or active groups on the surface of the sorbent. Due to the widespread use of chitosan and its derivatives as sorbent, it has become a necessity to investigate the surface properties. Thus, determining the surface characteristics of commercial chitosan with BET and SEM techniques has been the focus of this study.

2. Material and Method

2.1. Material supply

The chitosan used in the experiments was obtained from Adaga Food and Consulting Joint Stock Company operating in Antalya and is of commercial purity (Lot No: 070891). It was determined DD:80-85% and molecular weight:530-600 kDa by the manufacturer.

2.2. Surface characterization with SEM-EDX technique

Commercial chitosan samples were dried in an oven at 50 °C for 1 day before SEM analysis. Then, the gold-plated chitosan samples were analyzed in the ZEISS brand EvoMA10 model device.

2.3. Porosity analysis with BET technique

The surface porosity of chitosan samples was analyzed as a result of adsorption/desorption experiments carried out under a nitrogen atmosphere with a BET device (Micromeritics ASAP 2020). During the BET analysis, de-gas was applied to the chitosan sample at 60 °C for 12 hours. Thus, all volatile components including moisture in the content of chitosan were removed from the structure.

3. Results and Discussion

SEM images of the commercial chitosan sample are given in Figure 3. According to the 75 times magnified image, it is understood that commercial chitosan has a layered structure in the macro sense. However, in some parts of these layer fragments, a whitish sheen was noted. The presence of calcium (Ca) was detected in the structure as a result of the EDX analysis performed in a region that will include these whitish sheen. According to the spectrum obtained from the EDX analysis performed on the selected region in Figure 3(a), it was determined that the chitosan sample consisted of 32.5% C, 46% O, and 21.5% Ca. When looking at the 5000 times magnified image in the region where the white region is concentrated, it is clearly understood that the chitosan surface is covered with white particles. According to the result of EDX analysis performed in a narrower region in this image, the elemental composition was determined as 15.5% C, 48.5% O and 36% Ca. The obtained data show that there is a significant amount of Ca compound or mineral on the chitosan surface. The C content of chitosan decreased to 15% in regions where Ca concentration increased.

After the chitosan samples were washed three times with distilled water, they were dried in an oven at 50 °C and SEM images were examined again. The resulting image is given in Figure 4. According to this image, as a result of washing with pure water, it was noticed that the calcium particles on the chitosan surface decreased significantly and the chitosan surface was seen more clearly. According to the elemental composition obtained from the EDX spectrum, chitosan was determined to consist of 26.5% C, 46.5% O and 27% Ca. Elemental composition data also confirmed that the amount of Ca in the washed samples decreased and the C content increased.

Finally, while the chitosan samples were washed with distilled water, a few drops of diluted HCl solution was added to the washing water. It was similarly washed three times with acidified water and dried at 50 °C, and SEM images were taken again. According to the data obtained, it was observed that the calcium on the chitosan surface was completely removed as a result of pre-washing with acidified water. The data obtained from the EDX spectrum also confirmed that there was no residual Ca on the surface. In this context, the elemental composition was determined as 50.2% C, 44.5% O, and 5.3% N.

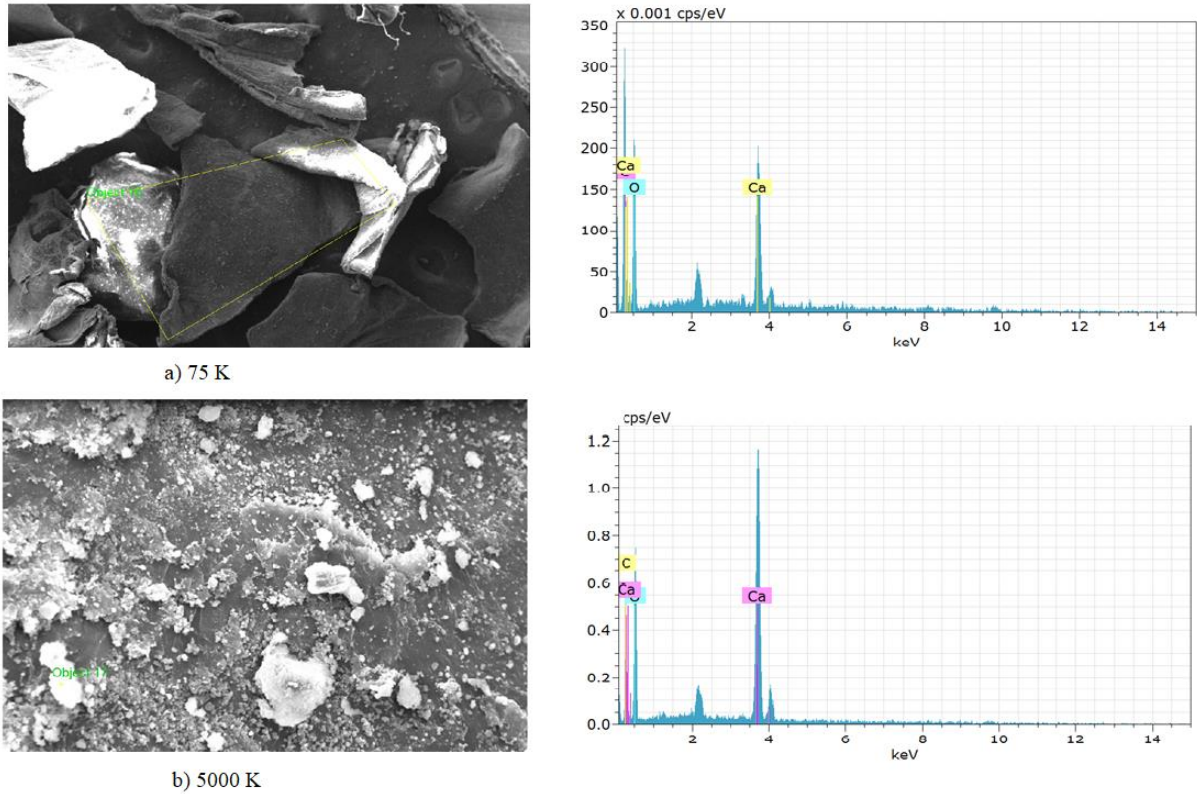


Figure 3. SEM images and EDX spectra of commercial chitosan

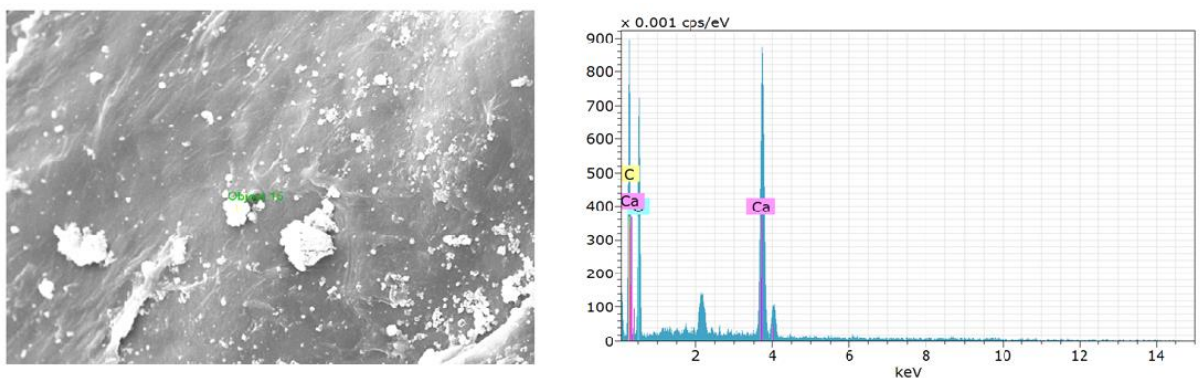


Figure 4. SEM image (x5000) and EDX spectrum of the chitosan sample washed with distilled water

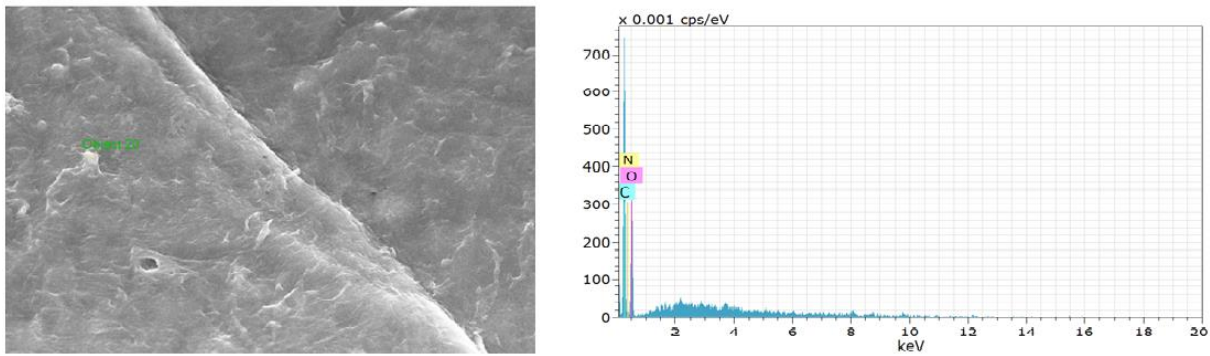


Figure 5. SEM image (x5000) and EDX spectrum of chitosan samples washed with acidified water

Commercial chitosan which was provided by the *Adaga Food and Consulting Joint Stock Company* in this study was produced from shrimp shells. It is possible to encounter minerals such as Ca and Mg in the shells of sea creatures such as shrimp. Although the demineralization step with HCl is applied in the production process of chitosan from these shells, some Ca remain in the structure of chitosan, since the demineralization efficiency is not 100%. In this study, pre-washing with dilute HCl solution can be considered as a second de-mineralization step. Thus, Ca, etc. minerals in the chitosan structure or surface can be completely removed.

The dissolution of chitosan in the acetic acid solution can be thought of as an acid-base reaction. Because chitosan can give all the reactions of amines by acting as an amine compound due to the active amine ($-\text{NH}_2$) groups in its structure [12]. Thus, the acetate salt of chitosan is formed as a result of the dissolution in the acetic acid medium. If there are mineral impurities such as Ca etc. on the chitosan surface, the formation of calcium acetate salt will be inevitable during the dissolution process. This situation causes both solvent loss and adverse effects in the modification process of chitosan with techniques such as intercalation and cross-link. Because the modification of chitosan takes place in the solution medium. In addition to these, in cases where chitin or chitosan is used directly as a sorbent, mineral impurities on the surface pass into the solution medium and cause contamination of the sorption medium due to the sorbent. All these reasons emphasize that mineral impurities such as Ca etc., which are a result of the low efficiency in the demineralization process, should be removed from the chitosan surface.

According to the SEM image in Figure 5, it is possible to say that the chitosan surface is non-porous, smooth, and membranous (like a membrane). The fact that chitosan is a non-porous material indicates that it performs its sorption efficiency, not through porosity, but through active amine and hydroxyl groups in its structure.

As a result of the adsorption/desorption experiments of chitosan samples under a nitrogen atmosphere with a BET device, the surface area was determined as $0.0632 \text{ m}^2/\text{g}$ and pore volume as $0.001255 \text{ cm}^3/\text{g}$. Moussout et al., (2018) [13] found the surface area of the chitosan sample, which has a DD of 82.5%, to be $0.1 \text{ m}^2/\text{g}$ in their study. The data obtained are in agreement with the literature.

In addition, the detection of the surface area as a very small value of $0.0632 \text{ m}^2/\text{g}$ also confirms the SEM images. The very low surface area due to porosity can be considered as another proof that chitosan is non-porous.

The data obtained within the scope of this study revealed that chitosan is a non-porous polymer. It also showed that there may be mineral layers such as calcium on the surface of commercially pure chitosan samples. If chitosan is to be used as an adsorbent in adsorption applications such as water softening, heavy metal removal, and sulfate removal, it is very important to pre-wash by using distilled water acidified with dilute HCl solution.

4. Acknowledgment

The study was supported by TÜBİTAK 1002 project program (Project number 218M695). We thank TÜBİTAK for its funding support.

5. Author Contribution Statement

In the study, Author 1 contributed to forming the idea, the analysis of the results, provision of the materials and examination of the results; Author 2 contributed making the design and literature review; Author 3 contributed to checking the spelling and checking the article in terms of content.

6. Ethics Committee Approval and Conflict of Interest

There is no need for any an ethics committee approval in the prepared article. However, funding support was received from TÜBİTAK.

7. References

- [1] Pillai CKS, Paul W, Sharma, CP. "Chitin and chitosan polymers: Chemistry, solubility and fiber formation". *Progress in Polymer Science*, 34, 641–678, 2009.
- [2] Sağ Y. "Investigation of the biosorption of heavy metal ions on chitin and chitosan". TÜBİTAK Report, Project Number: 199Y095, 2001.
- [3] Elibol M. "Production of chitin, chitosan, and derivatives from shellfish residues". TÜBİTAK Report, Project Number: 106M241, 2008.
- [4] Latańska I, Rosiak P, Paul P, Sujka W, Kolesińska B. *Modulating the Physicochemical Properties of Chitin and Chitosan as a Method of Obtaining New Biological Properties of Biodegradable Materials*. Editors: Berrade M. Chitin and Chitosan - Physicochemical Properties and Industrial Applications, 1-33, Intechopen, 2021.
- [5] Jin T, Liu T, Lam E, Moores A. "Chitin and chitosan on the nanoscale". *Nanoscale Horizons*, 6, 505-542, 2021.
- [6] Polat H. "Synthesis, characterization and comparative studies of toxic metal adsorption of chitin and chitosan biosorbents from pink shrimp (*Parapenaeus longirostris*) shell waste". TÜBİTAK Report, Project Number: 106T111, 2008.
- [7] Sonia TA. Sharma CP. *Chitosan and Derivatives for Drug Delivery Perspectives*. Editors: Jayakumar R, Prabakaran M, Muzzarelli A. Chitosan for Biomaterials I, 111-137, Springer Berlin, Heidelberg Advances in Polymer Science, 2011.
- [8] Cho YW. Jang J, Park CR, Ko SW. "Preparation and solubility in acid and water of partially deacetylated chitins". *Biomacromolecules*, 1, 609-614, 2000.
- [9] Kim YK, Jiang HL, Choi YJ, Park IK, Cho MH, Cho CS. "Polymeric nanoparticle of chitosan derivatives as DNA and siRNA carriers". *Advances in Polymer Science*, 243, 1-21, 2011.
- [10] Wu WC, Hsiao PY, Huang YC. "Effects of amylose content on starch-chitosan composite film and its application as a wound dressing". *Journal of Polymer Research*, 26, 137, 2019.
- [11] Kyzas GZ, Bikiaris DN, "Recent modifications of chitosan for adsorption applications: A critical and systematic review". *Marine Drugs*, 13, 312-337, 2015.
- [12] Darder M, Colilla M, Ruiz-Hitzky E. "Biopolymer-clay nanocomposite based on chitosan intercalated in montmorillonite". *Chemistry of Materials*, 15, 3774-3780, 2003.
- [13] Moussout H, Ahlafi H, Aazza M, Amechrouq A. "Bentonite/chitosan nanocomposite: Preparation, characterization and kinetic study of its thermal degradation", *Thermochimica Acta*, 659, 191-202, 2018.



Modeling the limiting performance of resistive superconductor fault current limiters for 2G HTS tape

Rezistif süperiletken arıza akımı sınırlayıcıların sınırlandırma performansının 2G HTS şerit için modellenmesi

Buğra YILMAZ^{1*}, Muhsin Tunay GENÇOĞLU²

^{1,2}Department of Electrical-Electronics Engineering, Faculty of Engineering, Firat University, Elazig, Turkey.

¹b.yilmaz@firat.edu.tr, ²mtgencoglu@firat.edu.tr

Received: 14.04.2022
Accepted: 06.05.2022

Revision: 28.04.2022

doi: 10.5505/fujece.2022.32042
Research Article

Abstract

Fault currents in power systems force valuable power system elements thermally, electro-dynamically and electromagnetically. Due to the increase in fault current levels, the installation of components resistant to fault currents and the damage of these currents to existing components bring economic problems. Therefore, various modern limiting methods have been developed in recent years. One of these methods, Resistive Superconducting Fault Current Limiter (R-SFCL), increases the security and sustainability of the system by eliminating these risks. This study made a dynamic model in MATLAB/Simulink by creating a sample R-SFCL in the laboratory using a 2G HTS (High-Temperature Superconductor) tape. With this model, the limitation analysis for single phase-ground fault is observed. The simulation results and the responses of the sample R-SFCL were compared and it was concluded that they showed a great deal of similarity.

Keywords: 2G HTS tape, Fault current limiting, Resistive SFCL, Simulation, Design.

Özet

Güç sistemlerindeki arıza akımları, değerli güç sistemi elemanlarını termal, elektro dinamik ve elektromanyetik olarak zorlamaktadır. Arıza akım seviyelerinin yükselmesi sebebiyle hem arıza akımlarına dayanıklı bileşenlerin tesisi hem de bu akımların mevcut bileşenlere zarar vermesi ekonomik problemleri beraberinde getirmektedir. Son yıllarda çeşitli modern sınırlandırma yöntemi geliştirilmiştir. Bu yöntemlerinden biri olan Rezistif Süperiletken Arıza Akım Sınırlayıcı (R-SFCL), bu riskleri ortadan kaldırarak sistemin güvenliğini ve sürdürülebilirliğini artırmaktadır. Bu çalışmada, 2G HTS (Yüksek Sıcaklıklı Süperiletken) şerit kullanılarak laboratuvar ortamında örnek bir R-SFCL oluşturularak MATLAB/Simulink'te dinamik bir modeli yapılmıştır. Bu model ile tek faz-toprak arızası için sınırlandırma analizi gözlemlenmiştir. Simülasyon sonuçları ile örnek R-SFCL'nin gösterdiği tepkiler karşılaştırılmış ve büyük oranda benzerlik gösterdikleri sonucuna varılmıştır.

Anahtar kelimeler: 2G HTS şerit, Arıza akımı sınırlandırma, Rezistif SFCL, Simülasyon, Tasarım.

1. Introduction

Increasing world population and industrialization have led to increased energy demand. New electricity generation, transmission and distribution systems are added to existing systems to meet the increasing demand for electrical energy. The increase in production capacity also increases the level of short-circuit currents. High-level fault currents can cause irreversible damage to power system elements. Therefore, power system breakers need to trip the fault current as soon as possible. Considering that the tripping capacity of typical high voltage breakers is limited to 80 kA, increased fault current levels will quickly exceed the capabilities of existing breakers [1]. Higher tripping capacity increases both the size and cost of breakers. Because of these situations, it is necessary to reduce the fault current quickly to non-hazardous levels. Many methods have been developed in recent years to limit the current. The series reactors added to the circuit limit the current, but they cause high voltage drop and power loss under normal operating conditions. While fuses called is-limiters do not cause power loss under normal conditions, they have the disadvantage of replacing the fuse after each short circuit

*Corresponding author

[2]. Superconducting Fault Current Limiters (SFCL), one of the modern fault current limiting methods, are a good solution for fault currents [3]. Elimination of fault currents and hazards is possible using SFCLs, which use the abrupt transition of superconducting material from the superconductor to the resistive region at a given critical current value [4]. SFCL causes low voltage drop and power loss at rated current. If critical values such as critical temperature (T_c), critical current density (J_c) and critical magnetic field (H_c) are exceeded, the resistance of the superconductor will increase [5].

After the short circuit is over, the SFCL cools down and returns to the superconducting region. SFCL can usually be isolated from the system during cooling by a circuit breaker [6]. SFCL can be classified into two different types in practice. These are Resistive SFCL and Inductive SFCL. R-SFCL is the ideal type due to its small size and reduced price of superconductors [7]. At the same time, R-SFCL reduces the effect of the DC factor of the fault current by lowering the X/R ratio and makes the breakers' work easier. It does not generate harmonics and does not cause magnetic field interference. R-SFCL applications in power systems have recently been preferred thanks to these advantages. Many superconducting materials are used in the R-SFCL design. These materials are divided into two groups according to their temperature: High-Temperature Superconductors (HTS) and Low-Temperature Superconductors (LTS). The HTS is cooled with liquid Nitrogen (LN_2) and has a critical temperature of over 30°K. This is a massive advantage over LTS materials, which operate at 4.2 °K, are very close to their critical temperature and are very sensitive to temperature changes. SFCL based on LTS has not been widely used as it requires a costly cooling system using liquid Helium (LHe) [8]. However, when using HTS for SFCL applications, cooling costs can be reduced ten times than LTS [9].

HTS materials are also divided into two groups 1G and 2G. 2G HTS materials have higher current carrying capacity, critical current level, magnetic flux value and mechanical strength. In addition, 2G materials pass into the resistive region faster than 1G materials [10]. Similarly, after the fault is complete, the 1G HTS returns to the superconducting region later than the 2G HTS. The 1G HTS has a lower normal operating resistance than the 2G HTS [11]. In brief, 2G HTS is an ideal choice for R-SFCL due to its high linear resistances, high current density and ability to operate in liquid nitrogen with low cryogenic costs [12]. In this paper, a sample R-SFCL application was created using 2G HTS tape in the laboratory, a dynamic model was developed in MATLAB/Simulink and the limitation analysis of 2G HTS materials was examined.

2. Materials and Method

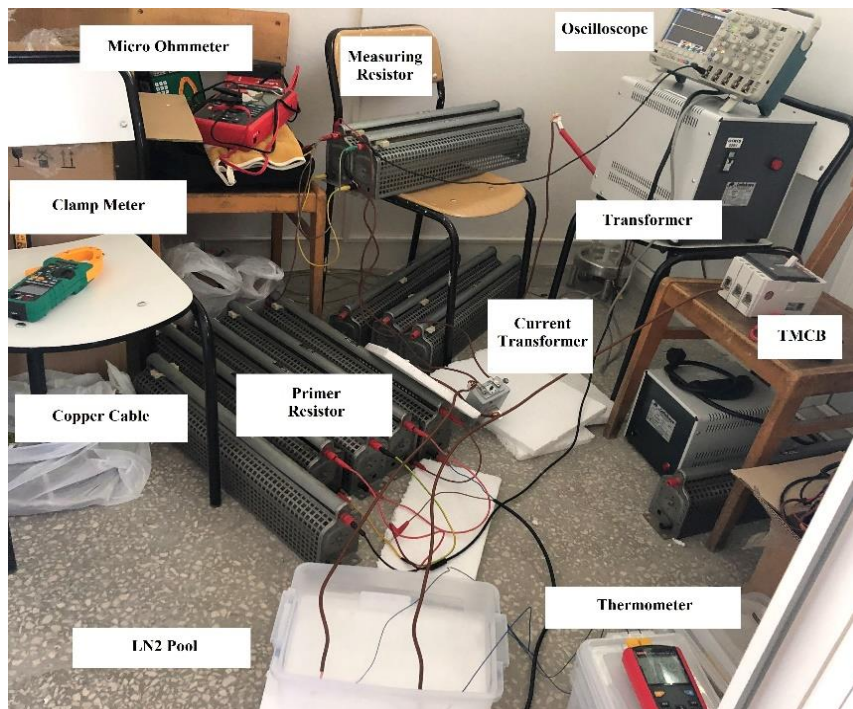
The system elements on which the tests were tested and the measurements were made are given in Table 1. To create the sample R-SFCL, a 2 m long 2G HTS tape produced by SuperPower company was divided into 40 cm lengths. The thickness of the superconducting tape is 6 mm and its critical current is 180 A. Details about the superconducting tape are given in Appendix A.

Table 1. System elements

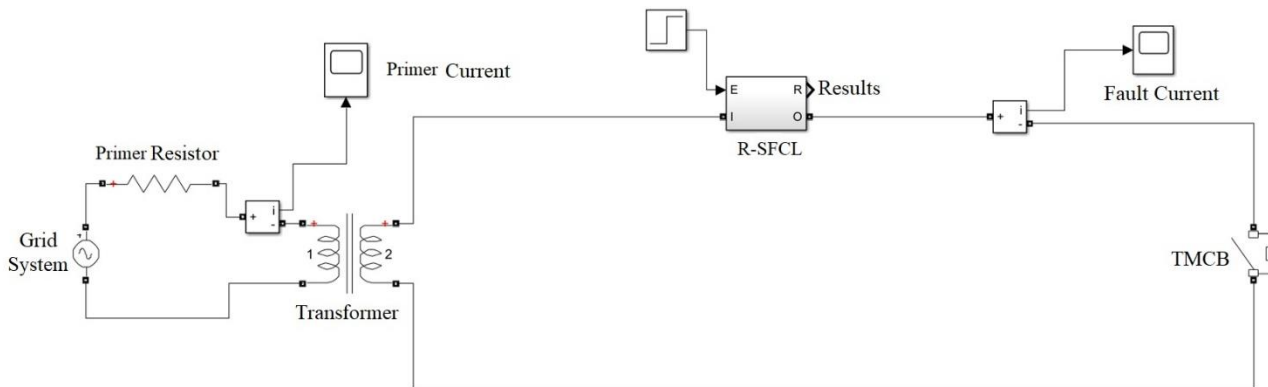
Element	Specification
Transformer	3 kVA, 220/5 V
Current Transformer	500/5 A
Thermal Magnetic Circuit Breaker (TMCB)	250 A
Primer Resistor	21.39 Ω
Measuring Resistor	1 Ω
Clamp Meter	USB Connected
Micro Ohmmeter	USB Connected
Thermometer	K Type Thermocouple USB Connected

Connections in the system were made with copper cable with a cross-section of 10 mm². The instantaneous short circuit current of the cable is 1 kA and its insulator is PVC. Since short circuit tests are carried out, the insulator must be resistant to high temperatures. The cable insulator used is temperature resistant up to 180 °C.

R-SFCL's LN₂ pool with a 6-liter plastic container. The container is soft plastic so that it does not crack in contact with LN₂. In addition, LN₂ was stored in a particular 10-liter cryogenic container. The overview of the test system is in Figure 1(a) and the Simulink model is shown in Figure 1(b).



(a)



(b)

Figure 1. (a) Test system (b) Simulink model

The current waveforms in the experiments were obtained by observing the voltage on the 1 Ω resistor on the oscilloscope screen. The current was also recorded instantaneously as an effective value with the help of a clamp meter. The temperature change of the superconductor during the failure was also instantly transferred to the computer with a K-type thermocouple thermometer. Superconducting tapes are soldered to one end of the copper plates to provide better transition resistance. Cable ends are connected to the other end of the copper plates. The fault was carried out with TMCB and 250 A was chosen to avoid damage to the superconducting tape. The superconductor connection with the copper plate is shown in Figure 2.



Figure 2. Superconducting tape connection with copper plate

2.1. Modeling

The current through the R-SFCL is less than the critical current value during normal operating conditions. Therefore, the resistance is close to zero and the R-SFCL conducts electricity almost without loss. However, in the event of a fault, the current exceeds the critical current value and the resistance of the superconducting material increases. Thus, the R-SFCL limits the fault current [13]. Briefly, R-SFCL, which produces a negligible voltage drop and power loss in normal operation, limits the fault current level with a nonlinear increase in resistance within the first half-period when the fault occurs.

R-SFCL model and simulations were performed in MATLAB-Simulink. The E-J curve of the superconducting material is based on the modeling [14-16]. In the R-SFCL model created in Simulink, the effective value of the system current is compared with the critical current value of the 2G HTS tape at any time. According to the E-J curve, there are three regions for the superconducting material: superconductivity, flux-flow and resistive. This curve is given in Figure 3. The resistance of R-SFCL for all three regions was calculated instantaneously by Equation 1. The current density was calculated by Equation 2.

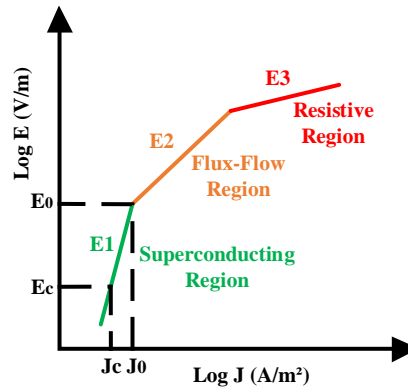


Figure 3. The E-J curve

$$R_{R-SFCL}(t) = \frac{E(J,T) \cdot L_s}{J(t) \cdot A_s} \quad (1)$$

$$J(t) = \frac{I_{R-SFCL}(t)}{A_s} \quad (2)$$

where, R_{Rsfcl} is the instant R-SFCL resistance (Ω), L_s is the superconductor length (m), A_s is the superconductor section (m^2), E is the electric field as a function of J and T (V/m), T is the instant R-SFCL temperature ($^{\circ}K$), I_{Rsfcl} is the instant R-SFCL current (A) and J is the instant current density (A/m^2).

2.2. Superconducting region

The R-SFCL current is below the critical value and the R-SFCL resistance is theoretically zero. E is calculated by Equation 3 [17-20].

$$E(J, T) = E_c \left(\frac{J}{J_c(T)} \right)^\alpha \quad (3)$$

$$J_c(T) = J_c \left(\frac{T_c - T}{T_c - T_0} \right) \quad (4)$$

$$\alpha_x = \frac{\log(E_0/E_c)}{\log \left((J_c/J_c(T))^{(1-\frac{1}{\beta})} (E_0/E_c)^{\frac{1}{\alpha}} \right)} \quad (5)$$

$$\alpha = \max[\beta, \alpha_x] \quad (6)$$

where, E_c is the critical electric field (1 $\mu\text{V}/\text{cm}$), $J_c(T)$ is the critical current density (A/m^2) as a function of T , J_c is the critical current density at 77 °K, T_c is the critical temperature (°K), T_0 is the first temperature value (77 °K), α_x is the time-varying value of the exponential value, α is the superconducting region exponent value, the α value ranges from 5-15 for 1G HTS materials and 15-40 for 2G HTS materials [19], [21], [22].

2.3. Flux-flow region

Exceeding the critical current increases the R-SFCL resistance as the electric field increases and the current is limited. The temperature rises and the rising temperature lowers $J_c(T)$, so the electric field increases continuously. E is calculated by Equation 7 [5, 18, 23].

$$E(J, T) = E_0 \cdot \left(E_c/E_0 \right)^{\beta/\alpha} \frac{J_c}{J_c(T)} \left(J/J_c \right)^\beta \quad (7)$$

where, E_0 is the electric field during the transition from the superconducting region to the flux-flow region (V/m) and takes a value between 0.1 and 1 V/m , β is the exponent of the flux-flow region, for both 1G and 2G HTS materials range from 2-4 [19], [21], [22].

2.4. Resistive region

As soon as the temperature exceeds the critical temperature, R-SFCL is no longer superconducting. R-SFCL resistance and E vary with J and T . E is calculated by Equation 8 [5, 18, 23].

$$E(J, T) = \rho(T_c) J \frac{T}{T_c} \quad (8)$$

where, $\rho(T_c)$ is the superconductor resistivity in the resistive region ($\Omega \cdot \text{m}$).

During this process, the superconducting material heats up. After a recovery time, the cryogenic system cools the superconducting material and returns to the R-SFCL superconducting region. There is continuous heat transfer between the LN_2 and the superconducting tape during and after the limiting process. The heat transfers between LN_2 and superconducting material and R-SFCL temperature change were calculated with Equations 9, 10, 11, 12 and 13, respectively [5, 17, 18, 23-26].

$$Q_{Rsfcl}(t) = \int I_{Rsfcl}(t)^2 R_{Rsfcl}(t) dt \quad (9)$$

$$Q_{cryosys}(t) = \int \left(\frac{T(t)-T_0}{\theta_s} \right) dt \quad (10)$$

$$\theta_s = \frac{1}{k L_s \pi d_s} \quad (11)$$

$$T_{Rsfcl} = T_{Rsfcl} + (Q_{Rsfcl} - Q_{cryosys})/c_s \quad (12)$$

$$c_s = L_s A_s c_{vol} \quad (13)$$

where, Q_{Rsfcl} is the heat energy emitted by the R-SFCL (J), $Q_{cryosys}$ is the heat energy received by the cryogenic system (J), θ_s is the thermal resistance between R-SFCL and cryogenic system (K/W), k is the heat transfer coefficient to the cryogenic system (W/Km²), d_s is the superconductor diameter (m), c_s is the superconductor heat capacity (J/K), c_{vol} is the superconductor volumetric specific heat (J/Km³), T_{Rsfcl} is the R-SFCL instant temperature (°K).

All equations were created as M-function in Simulink according to the algorithm flow chart in Figure 4.

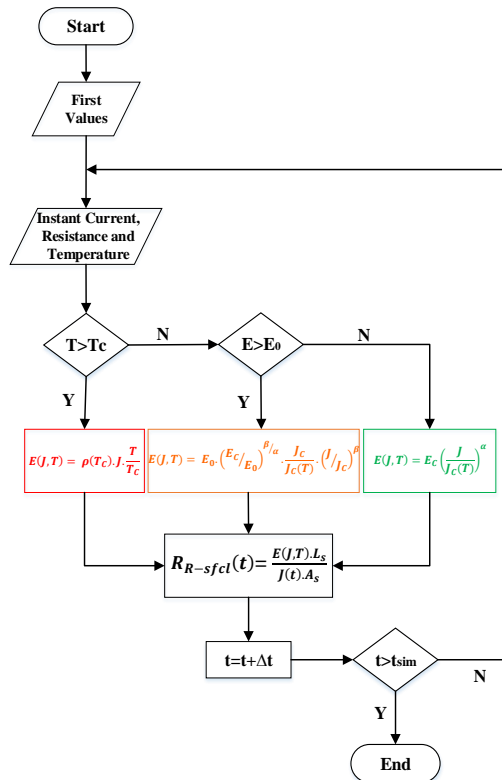


Figure 4. The algorithm flow chart

3. Results

This section observed R-SFCL responses with a fault current of 189 A_{rms}. At the same time, the same fault situation was simulated in the model that created it and the results were examined. A short circuit current of 189 Arms was provided with a primary resistance of 21.39 Ω added to the transformer primary to perform the limitation analysis. First of all, the

fault current was observed for the absence of R-SFCL in the experimental system. Figure 5 shows the fault current waveform measured over a 500/5 A current transformer and a 1 Ω measuring resistor. Figure 6 also shows the fault current with R-SFCL.



Figure 5. Fault current in the system without R-SFCL



Figure 6. Fault current in the system with R-SFCL

As seen in Figure 5, the peak value of the current was 2.6 A. Since the current transformer ratio is 100, the real peak value of the fault current in the system without R-SFCL was 260 A. When R-SFCL, which used only 40 cm 2G HTS tape, was added to the system for the same fault, the real peak value became 244 A and decreased by 16 A.

In the simulations performed with the model created in MATLAB/Simulink, the fault currents for the system without R-SFCL and with R-SFCL were shown in Figures 7 and 8, respectively.

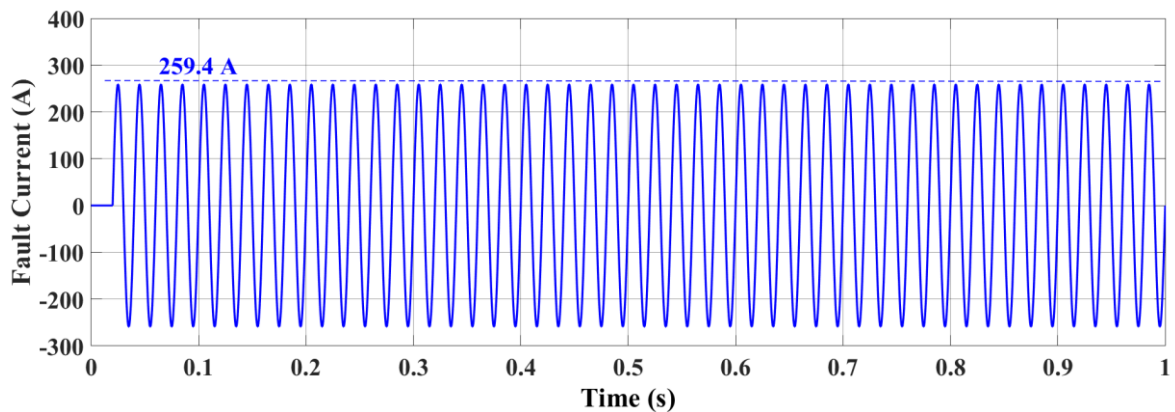


Figure 7. Fault current in the system without R-SFCL

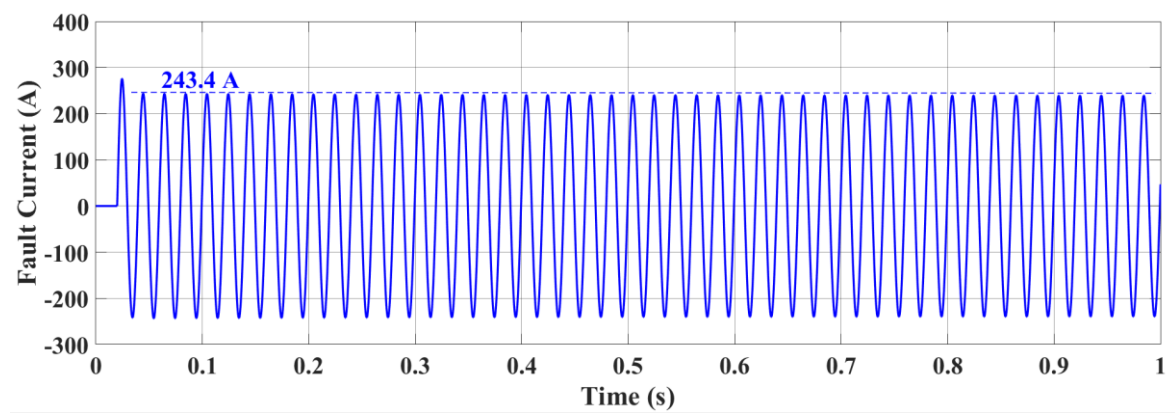


Figure 8. Fault current in the system with R-SFCL

As seen in the simulation results, the peak values of the fault current for both the case without R-SFCL and with R-SFCL were close and consistent with the test results. From the voltage and current data measured during the fault, it has been seen that the fault resistance varies between $7 \text{ m}\Omega$ and $7.1 \text{ m}\Omega$. While the nominal resistance of the tape was $876.404 \mu\Omega$, it increased approximately 8.1 times with the fault. Finally, the resistance change observed in the model created is shown in Figure 9 and it is quite close to the experimental result.

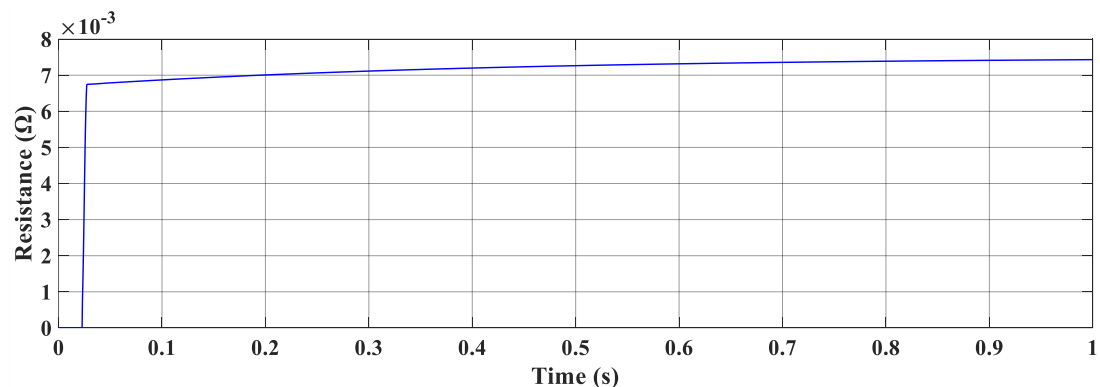


Figure 9. R-SFCL resistance

The rapidly increasing resistance value at the time of fault also caused an increased temperature and the temperatures at the points where the K-type thermocouple terminals were connected varied between $77\text{-}340 \text{ }^\circ\text{K}$. After reaching these

temperature values, the tape must be cooled quickly and effectively. As a matter of fact, in some experiments, the superconducting tapes were damaged and burned. Examples of damaged superconducting tapes are shown in Figure 10.



Figure 10. Damaged superconducting tapes

The reason for this situation is the Hot-Spot event. Hot-Spot is due to the inhomogeneity of the critical current distribution on the tape surface. The tapes were irreversibly damaged as a result of the Hot-Spot. Manufacturers and developers use the thick silver layer and Hastelloy C276 layer throughout the superconducting material to solve this problem [27]. With the addition of these layers with high resistive properties, the thermal mass of the superconducting tape, whose linear resistance decreases, will increase [28]. Other ways to circumvent the Hot-Spot issue are still in development today. One is to use a sapphire-based substrate, while the other is to change the architecture of the tape. A closed-loop cooling system will also minimize the possibility of Hot-Spot occurrence. In this study, since it is an open-loop cooling system, the occurrence of Hot-Spot was inevitable according to the fault time and current level. At the same time, the cable-connected parts of the copper plates that are soldered to the strips remain outside the liquid nitrogen. This part, which is directly at room temperature, also causes rapid evaporation of liquid nitrogen. This situation is similar to current leads in real R-SFCL applications. The current leads are one of the R-SFCL's most significant design issues because they directly reduce the cooling capacity.

4. Conclusions

In this study, a laboratory sample of R-SFCL used a 40 cm long 2G HTS tape was made and this sample was modeled in MATLAB/Simulink. Experiment and simulation results were compatible with each other and R-SFCL reduced the peak value of fault current by 16 A. This tape, which causes negligible power loss and voltage drop by showing resistance of about $880 \mu\Omega$ in the nominal operating condition, limited the fault by showing resistance of $7 \text{ m}\Omega$ during the fault. Future studies will examine the effects of winding shapes on efficiency and limitation analyses by supplying longer tapes.

5. Acknowledgments

This study was supported by Firat University Scientific Research Foundation (Project Numbers MF.20.02).

6. Author Contribution Statement

In this study, Author 1 contributed to the creation of the idea, the design and the literature review, the evaluation of the results obtained, the procurement of the materials used and the analysis of the results; Author 2 contributed to the creation of the idea, spelling, the procurement of the materials used, reviewing the results and checking the paper for content.

7. Ethics Committee Approval and Conflict of Interest

There is no need for an ethics committee approval in the prepared article. There is no conflict of interest with any person/institution in the prepared article.

8. References

- [1] Seyedi H, Tabei B. “Appropriate placement of fault current limiting reactors in different hv substation arrangements”. *Circuits Syst.*, 03, 03, 252–262, 2012.
- [2] Kempinski A, Rusinski J, Hajdasz S. “Analysis of Recovery Time of HTS tapes with electrical insulation layers for superconducting fault current limiters under load conditions”. *IEEE Trans. Appl. Supercond.*, 29, 8, 2019.
- [3] Blair SM, Booth CD, Burt GM. “Current-time characteristics of resistive superconducting fault current limiters”. *IEEE Trans. Appl. Supercond.*, 22, 2, 2012.
- [4] M. C. Nagarathna V. M. H. and S. R., “A Review on Super Conducting Fault Current Limiter (SFCL) in power system,” 3, 2, 485–489, 2015.
- [5] Zhang X, Ruiz HS, Zhong Z, Coombs TA. “Implementation of resistive type superconducting fault current limiters in electrical grids : performance analysis and measuring of optimal locations”. *Superconductivity*, 4, 1-6, 2015.
- [6] Gorbunova DA, Kumarov DR, Scherbakov VI, Sim K, Hwang S. “Influence of polymer coating on SFCL recovery under load”. *Prog. Supercond. Cryog.*, 12, 1, 44–47, 2020.
- [7] Zhu J, Zhao Y, Chen P, Gong J, Jiang S, Wang S. “Performance analysis on a flux coupling superconducting fault current limiter (SFCL) considering the power grid integration based on MATLAB / SIMULINK”. *2018 IEEE Int. Conf. Appl. Supercond. Electromagn. Devices*, 3, 1–2, 2018.
- [8] Ignatius OK. “Transient stability improvement using resistive-type superconducting fault current limiters (R-SFCL)”. *Int. J. Eng. Technol. Sci.*, 6, 2, 28–41, 2019.
- [9] Zenitani Y, Akimitsu J. “Discovery of the new superconductor MgB₂ and its recent development”. *Oyobuturi*, 71, 1, 17–22, 20027.
- [10] Kim JS, Lim SH, Kim JC. “Study on application method of superconducting fault current limiter for protection coordination of protective devices in a power distribution system”. *IEEE Trans. Appl. Supercond.*, 22, 3, 4–7, 2012.
- [11] Kulkarni S, Dixit M, Pal K. “Study on recovery performance of high T_c superconducting tapes for resistive type superconducting fault current limiter applications”. 36, 1231–1235, 2012.
- [12] Zampa A, Holleis S, Badel A, Tixador P, Bernardi J, Eisterer M. “Influence of local inhomogeneities in the REBCO layer on the mechanism of quench onset in 2G HTS Tapes”. *IEEE Trans. Appl. Supercond.*, 32, 3, 2022.
- [13] Moyzykh M. *et al.* “First Russian 220 kV superconducting fault current limiter for application in city grid”. *IEEE Trans. Appl. Supercond.*, 31, 5, 1–7, 2021.
- [14] Hatata AY, Ebeid AS, El-Saadawi MM. “Application of resistive super conductor fault current limiter for protection of grid-connected DGs”. *Alexandria Eng. J.*, 57, 4, 4229–4241, 2018.
- [15] De Sousa WTB, Polasek A, Dias R, Matt CFT, De Andrade R. “Thermal-electrical analogy for simulations of superconducting fault current limiters”. *Cryogenics (Guildf)*, 62, 97–109, 2014.
- [16] Chen Y, Li S, Sheng J, Jin Z, Hong Z, Gu J. “Experimental and numerical study of co-ordination of resistive-type superconductor fault current limiter and relay protection”. *J. Supercond. Nov. Magn.*, 26, 11, 3225–3230, 2013.
- [17] Blair S.M, Booth CD, Burt GM. “Current-time characteristics of resistive superconducting fault current limiters”. *IEEE Trans. Appl. Supercond.*, 22, 2, 5600205, 2012.
- [18] Nemdili S, Belkhiat S. “Modeling and simulation of resistive superconducting fault-current limiters”. *J. Supercond. Nov. Magn.*, 25, 7, 2351–2356, 2012.
- [19] Dutta S, Babu BC. “Modelling and analysis of resistive Superconducting Fault Current Limiter”. *IEEE TechSym 2014 - 2014 IEEE Students’ Technol. Symp.*, 362–366, 2014.
- [20] Liang H, Chen Y, Duan R, Lu Y, Sheng J. “Numerical Study on the on-grid performance of superconducting cable cooperated with R-SFCL”. *IEEE Trans. Appl. Supercond.*, 32, 4, 2022.
- [21] Qian K, Guo Z, Terao Y, Ohsaki H. “Electromagnetic and thermal design of superconducting fault current limiters for DC electric systems using superconducting”. 2017.
- [22] Manohar P, Ahmed W. “Superconducting fault current limiter to mitigate the effect of DC line fault in VSC-HVDC system”. *2012 Int. Conf. Power, Signals, Control. Comput.*, 1–6, 2012.
- [23] Xue S, Gao F, Sun W, Li B. “Protection principle for a DC distribution system with a resistive superconductive fault current limiter”. *Energies*, 8, 6, 4839–4852, 2015.

[24] Elmitwally A. “Proposed hybrid superconducting fault current limiter for distribution systems”. *Int. J. Electr. Power Energy Syst.*, 31, 10, 619–625, 2009.

[25] Langston J, Steurer M, Woodruff S, Baldwi T, Tang J. “A generic real-time computer simulation model for superconducting fault current limiters and its application in system protection studies”. *IEEE Trans. Appl. Supercond.*, 15, 2 PART II, 2090–2093, 2005.

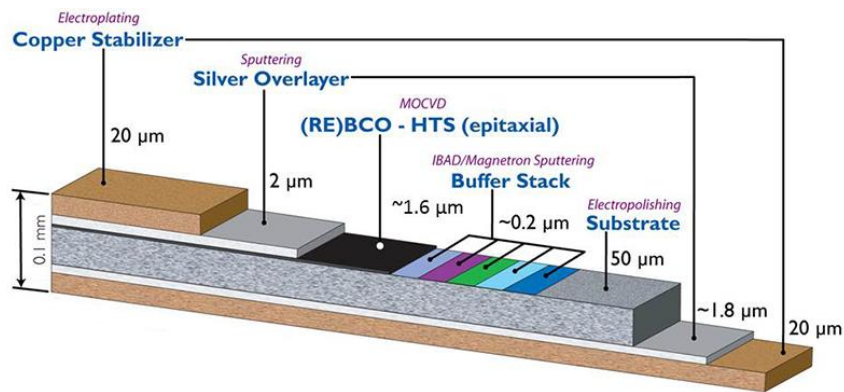
[26] Zhu J, Chen S, Jin Z. “Progress on second-generation high-temperature superconductor tape targeting resistive fault current limiter application”. *Electron.*, 11, 3, 2022.

[27] Escamez G, Vialle J, Bruzek CE, Grose V, Bauer M, Tixador P. “Numerical investigations of ReBCO conductors with high limitation electric field for HVDC SFCL”. *IEEE Trans. Appl. Supercond.*, 28, 4, 2018.

[28] Badel A, Escamez G, Tixador P. “REBCO FCL modelling: Influence of local critical current non-uniformities on overall behavior for various tape architectures”. *IEEE Trans. Appl. Supercond.*, 25, 3, 13–16, 2015.

Appendix A

Tape Structure



Tape Properties

	Minimum I_c measured by continuous direct current	Width	Total Wire Thickness	Critical Axial Tensile Strain at 77K	Critical Bend Diameter in Tension (40μm) @ room temp	Critical Bend Diameter in Compression (40μm) @ room temp
SCS6050	150 amp	6 mm	0.1 mm	0.45%	11 mm	11 mm



Characterization of polyurethane produced by polyol synthesized from corn oil

Mısır yağından sentezlenen poliolden üretilen poliüretanın karakterizasyonu

Ercan AYDOĞMUŞ^{1*} , Fethi KAMIŞLI² 

^{1,2}Department of Chemical Engineering, Faculty of Engineering, Firat University, Elazığ, Turkey.

¹ercanaydogmus@firat.edu.tr, ²fkamisli@firat.edu.tr

Received: 26.03.2022

Accepted: 18.04.2022

Revision: 11.04.2022

doi: 10.5505/fujece.2022.36855

Research Article

Abstract

In this study, biopolyol has been synthesized from corn oil by epoxidation, hydroxylation, neutralization, and purification processes. The rheological properties of both corn oil and polyol obtained from corn oil have been compared. When the variation of viscosity with temperature is examined, it is seen that corn oil-based polyol is more viscous than corn oil. Accordingly, it is thought that the molecular structure of the biopolyol changes, and its molecular weight increases. According to the results obtained, the hydroxyl number of the synthesized polyol is determined as approximately 160 mg KOH/g polyol by the analytical method. The produced polyols have been prepared for polyurethane production after being characterized physically and chemically. The production of polyurethane sponge with a suitable process and method has been realized according to the purpose of use. The approximate density of the produced polyurethane was 40 kg/m³ and the thermal conductivity coefficient was found to be 0.026 W/m·K. Also, Taguchi method has been used in experimental studies to determine an efficient and economical process in both the polyol synthesis and the polyurethane production.

Keywords: Corn oil, Polyol, Polyurethane, Rheology, Characterization.

Özet

Bu çalışmada mısır yağından epoksilleme, hidrosilleme, nötralizasyon ve saflaştırma işlemiyle biopoliol sentezlenmiştir. Mısır yağından elde edilen polioli ve mısır yağının reolojik özellikleri karşılaştırılmıştır. Viskozitenin sıcaklıkla değişimi incelendiğinde mısır yağı esaslı polioliün mısır yağına göre daha viskoz olduğu görülmektedir. Buna göre biopolioliün moleküler yapısının değiştiği ve molekül ağırlığının arttığı düşünülmektedir. Elde edilen sonuçlara göre sentezlenen polioliün hidroksil sayısı yaklaşık 160 mg KOH/g polioli olarak analitik yöntemle tayin edilmiştir. Üretilen polioller, fiziksel ve kimyasal olarak karakterize edildikten sonra poliüretan üretimi için hazırlanmıştır. Kullanım amacına göre poliüretan süngerin uygun bir proses ve yöntemle üretimi gerçekleştirilmiştir. Üretilen poliüretanın yaklaşık yoğunluğu 40 kg/m³ ve ısı iletkenlik katsayısı 0.026 W/m·K olarak bulunmuştur. Ayrıca deneysel çalışmalarda hem polioli sentezinde hem de poliüretan üretiminde verimli ve ekonomik bir süreç belirlemek amacıyla Taguchi yöntemi kullanılmıştır.

Anahtar kelimeler: Mısır yağı, Polioli, Poliüretan, Reoloji, Karakterizasyon.

1. Introduction

Today, the use of biopolymer raw materials is becoming more and more widespread. In particular, the synthesis of bioraw materials can be realized by using renewable resources and wastes. For example, polyol, which is the raw material of polyurethane, is obtained from vegetable oils instead of petrochemical sources. Studies have shown that triglycerides in the structure of vegetable oils are suitable for polyol production.

The mechanical properties of high-density and rigid polyurethane foams have been studied in the literature [1]. The determination of mechanical, structural, and morphological properties of polyurethane foams is an important research topic [2]. In the current studies, soybean oil-based polyol was obtained by applying epoxidation and hydroxylation steps to soybean oil. The properties of soy-based polyol and polyurethane were examined and their characterizations were made.

*Corresponding author

Besides, the variation of viscosity, density, and molecular weight of polyol obtained from soybean oil with temperature was determined [3].

As a result of the modification of vegetable oils, both the double bonds in their molecules are broken and their molecular weights increase. For these reasons, an increase in the viscosity of polyols synthesized from vegetable oils can be observed compared to vegetable oils. Also, when the rheological properties of vegetable oils and polyols obtained from them are examined, it has been determined that the viscosity values decrease as the temperature increases [5-7].

It has been observed that the heat transfer coefficients of castor oil-based polyurethane materials are lower than commercial polyurethane materials. From TGA curves, it has been determined that the thermal stability of castor oil-based polyurethane materials is better than the polyurethanes produced from the commercial polyol. From the mechanical strength test results, it was observed that the mechanical properties of castor oil-based materials were weakened compared to the commercial product [4].

In this study, polyol, the raw material of polyurethane, has been synthesized from corn oil by economical methods. After examining the physical and chemical properties of the obtained biopolyol, it has been used in the production of polyurethane. The unique aspect of this research is both the synthesis of bioraw materials and the production of polyurethane foam with the raw material obtained. The mechanical properties, thermal conductivity coefficient, density, thermal stability, and surface morphology of polyurethane produced from corn oil-based polyol have been evaluated.

2. Materials and Methods

2.1. Materials

The corn oil used has 30 % monounsaturated, 57 % polyunsaturated, and 13 % saturated fat. Besides, the density of corn oil at room temperature is 910 kg/m^3 and its viscosity is 74 cp. Refined corn oil used in experimental processes has a density of 910 kg/m^3 at $25 \text{ }^\circ\text{C}$, a refractive index of 1.45, an iodine index of 105, and a saponification number of 170. The density of the used filler (CaF_2) is 3180 kg/m^3 , and the particle diameter is below about $5 \text{ }\mu\text{m}$. Hydrogen peroxide (H_2O_2) 30 %, methanol (CH_3OH) 99.5 %, acetic acid (CH_3COOH) 80 %, sulfuric acid (H_2SO_4) 95–98 % were supplied from Merck. Toluene diisocyanate, triethylenediamine, silicon, and tin octoate have been obtained from Ravago Petrochemicals.

2.2. Experimental method

In this research, biopolyol has been synthesized from corn oil by epoxidation, hydroxylation, purification, and neutralization processes. After using optimum amounts of corn oil and acetic acid in PID-controlled reactor (Figure 1), hydrogen peroxide was added dropwise. Hydroxylation of the synthesized epoxy-corn oil was achieved with the help of methanol. This process was carried out using certain amounts of methanol, water, and sulfuric acid. In the last stage, impurities such as water and methanol were recovered with the help of a vacuum rotary evaporator. After this stage, the neutralization process was carried out again and the phases were separated from each other with the help of a separating funnel to obtain the biopolyol [11].



Figure 1. Polyol synthesis system (PID) from corn oil

In the production of polyurethane, it was mixed with corn oil-based polyol filler (CaF_2) for 5 minutes at a mixing speed of 750 rpm. After adding certain proportions of water, silicon, and amine mixture to the polyol, TDI was added and mixed at 1500 rpm for 2 minutes. After pouring the mixture into the prepared molds, it was waited for 24 hours to cure. Then the physical characterization of the polyurethane was done.

3. Results and Discussions

3.1. Rheological properties of corn oil and its polyol

The rheological properties of corn oil in Figure 2 and corn oil-based polyol in Figure 3 at different temperatures are shown. Corn oil-based polyol has higher viscosity and shear stress than corn oil. This change can occur due to the increase in both the molecular weight and the molecular chain length. When the rheological properties of corn oil and polyol obtained from corn oil were examined, it was determined that the temperature increase decreased the viscosity. Besides, shear-thinning behavior has been observed in both corn oil and polyol obtained from corn oil. Fluids with such rheological behavior (non-Newtonian) show pseudoplastic behavior [8].

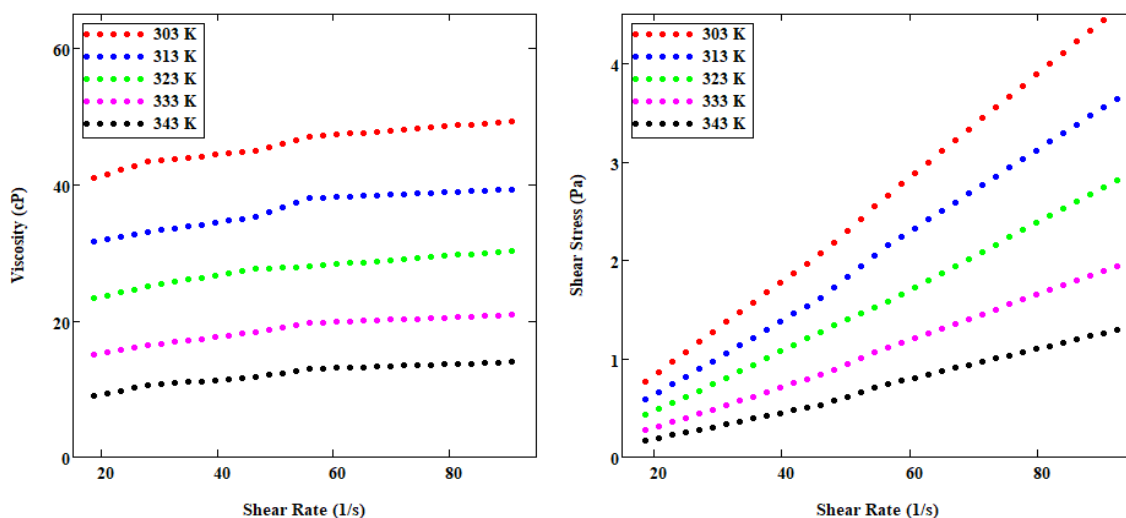


Figure 2. Variation of viscosity and shear stress of corn oil with shear rate at different temperatures

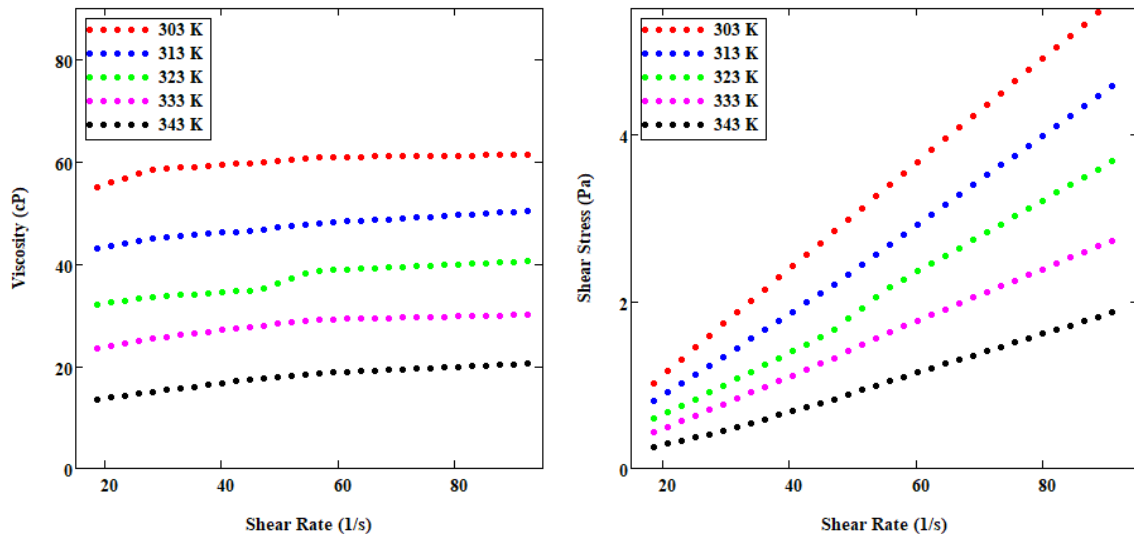


Figure 3. Variation of viscosity and shear stress with shear rate of corn oil-based polyol

3.2. FTIR spectra of corn oil and polyol

Corn oil-based polyol has been synthesized by changing the structure of refined corn oil. The chemical bond structure of both corn oil and synthesized polyurethane have been determined by FTIR spectrophotometer. In particular, the presence of hydroxyl bonds in the structure of the corn oil-based polyol indicates that the modification is successful. Figure 4 shows 1236-1099 cm^{-1} C-O ester groups, 1647 cm^{-1} C=C cis-olefins, 1745 cm^{-1} ester carbonyl groups of triglycerides, 3009 cm^{-1} C-H bonds, 2923-2855 cm^{-1} CH_2 groups vibration stresses in FTIR spectra of corn oil.

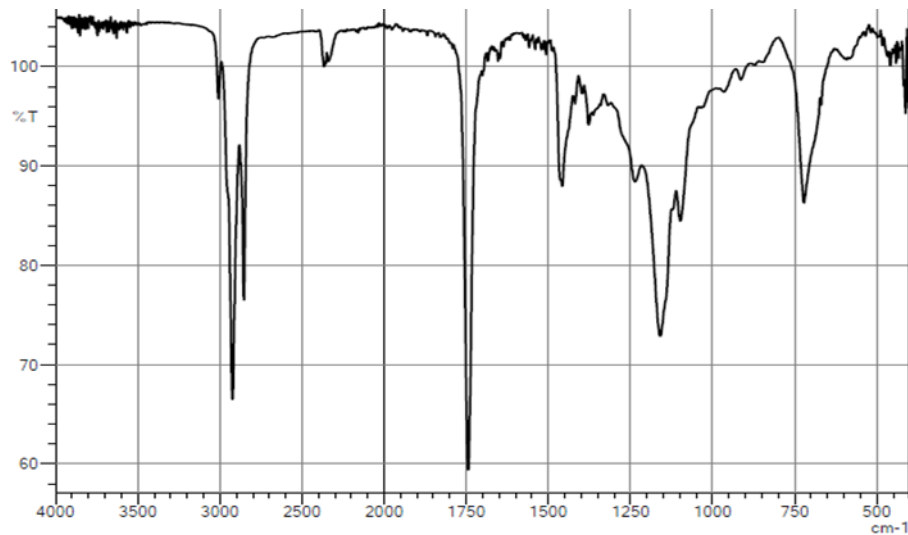


Figure 4. FTIR spectra of corn oil

In FTIR spectra in Figure 5, 3498 cm^{-1} OH stretching vibrations, 3293 cm^{-1} NH stretching vibrations, 2970 cm^{-1} CH asymmetric stretching vibrations, 2866 cm^{-1} CH symmetrical stretching vibrations, 2273 cm^{-1} N=C=O stretching vibrations, 1720 cm^{-1} C=O stretching vibrations, 1535 cm^{-1} NH bending vibrations, 1452 cm^{-1} CH shear vibrations, 1223 cm^{-1} CN and 1094 cm^{-1} CO stretching vibrations are shown.

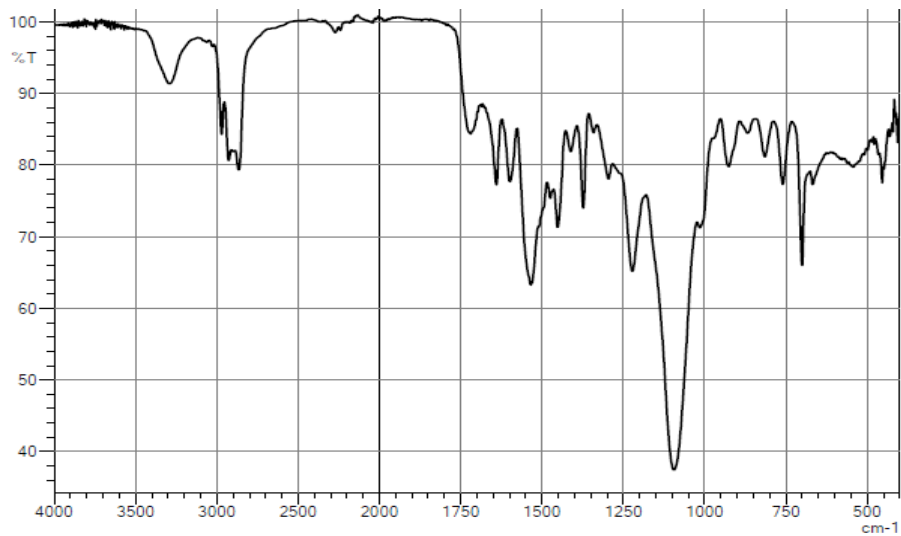


Figure 5. FTIR spectra of polyurethane derived from corn oil-based polyol

3.3. Tensile test of polyurethane produced from corn oil-based polyol

Standard samples have been prepared for polyurethane and measurements are made in the tensile test device. Samples were prepared in standard molds with the cross-sectional area ($a = 20 \text{ mm}$, $b = 10 \text{ mm}$, and $A = 200 \text{ mm}^2$) and length ($L = 100 \text{ mm}$). The applied preload, the tensile speed of 10 mm/minute , the stress ($\sigma = \text{N/mm}^2$), and the elongation ($\epsilon = \text{mm}$) of the sample were determined. The polyurethane obtained from corn oil-based polyol was cut into standard sizes and prepared for the tensile test. A force of 10 mm/minute was applied to the standard sample with an initial length of 100 mm and a cross-sectional area of 200 mm^2 ($20 \text{ mm} \cdot 10 \text{ mm}$). The maximum stress reached up to about 100 kPa . As seen in Figure 6, approximately 75% elongation was observed in the standard sample relative to its initial length. The tensile test started with a preload of 5 N and the maximum force was measured as approximately 20 N .

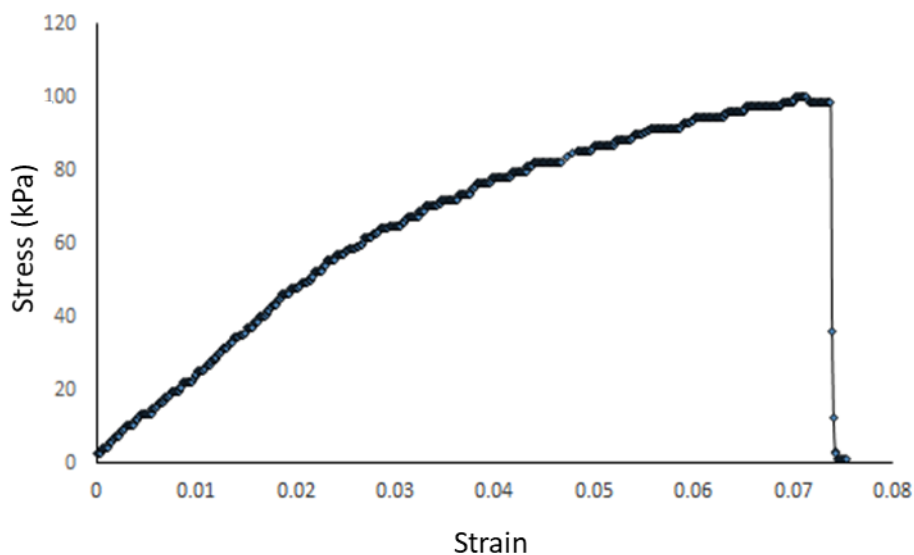


Figure 6. Deformation of corn oil-based polyurethane due to applied force

3.4. SEM image of polyurethane

SEM image and EDX data of polyurethane obtained from corn oil-based polyol are given in Figure 7. As seen here, carbon is 66.89 wt.%, oxygen 26.61 wt.%, nitrogen 3.28 wt.%, fluorine 2.98 wt.% and tin 0.23 wt.%. Catalysts used in EDX data may be slightly removed. After the conditions are optimized, there is no significant change in the amount of catalyst used. Compounds such as CaF_2 , which are called fillers and additives, have been used to increase the density, non-flammability, and thermal stability of polyurethane. Before the reaction, the additives must be mixed or mixed homogeneously with the polyol. Use of the additive more than 30 g per 100 g of vegetable oil-based polyol: It affects the mechanical strength, thermal conductivity coefficient, and pore structure negatively.

Besides, the high use of additives increases the number of closed cells and makes breathing between cells difficult. The more regular the pore structure of the obtained polyurethane, the lower the thermal conductivity coefficient. As the porosity and the number of independent cells increase, the insulation property of polyurethane improves. Especially when the SEM images are examined, the surface morphology and pore structure of the polyurethane can be determined [9].

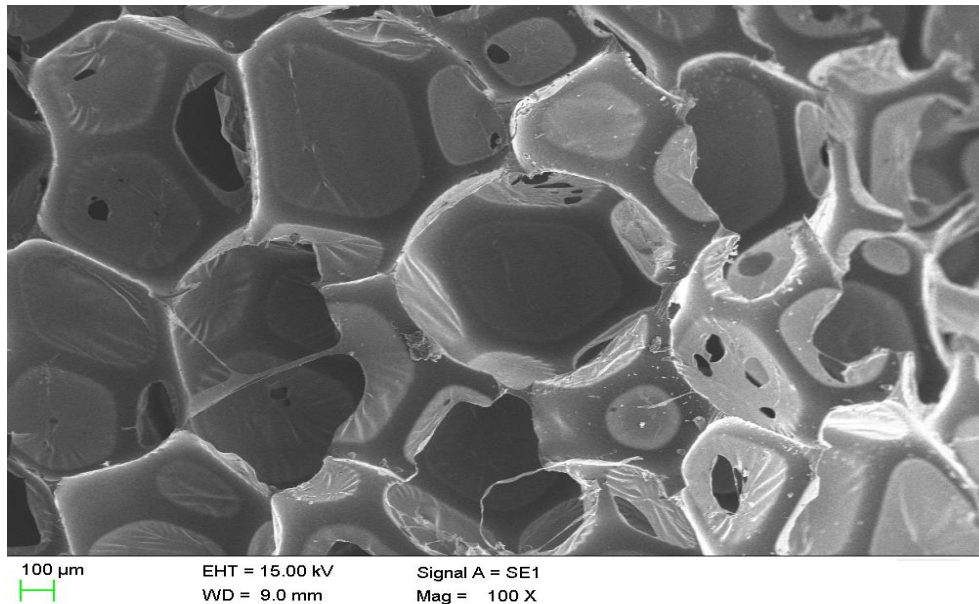


Figure 7. SEM image of polyurethane obtained from corn oil-based polyol

3.5. Thermogravimetric analysis (TGA) of polyurethane

TGA analyzes have been carried out at a nitrogen gas flow rate of 100 mL/min, starting at 20 °C, with a heating rate of 10 °C/min, using an alumina crucible up to a temperature of 600 °C. TGA curve of polyurethane produced with polyol synthesized from corn oil is shown in Figure 8. When TGA curve of the polyurethane obtained from corn oil-based polyol is examined, it is seen that physical impurities are removed in the first region. It is seen that the chemical decomposition of polyurethane started at a temperature of approximately 275 °C. The thermal degradation behavior of the polymer occurred rapidly in the second region. After the temperature of 400 °C (third region), thermal decomposition structures are observed more slowly.

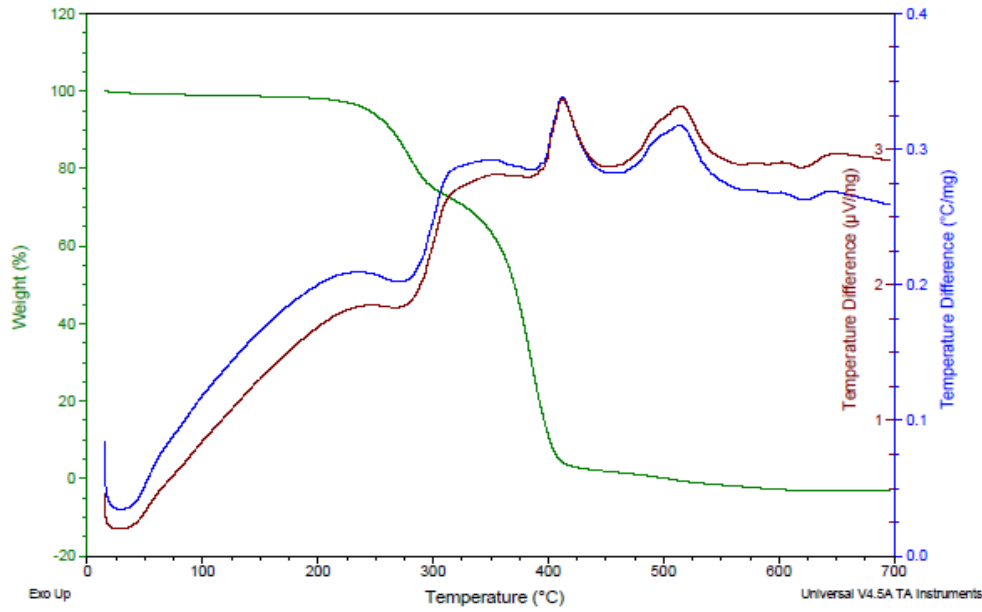


Figure 8. TGA curve of polyurethane produced from corn oil-based polyol

4. Conclusions

In this study, biopolyol has been synthesized from corn oil, and its physical and chemical characterization is carried out. In FTIR results, it is seen that the double bonds in the vegetable oil are broken and hydroxyl is attached to the structure [10]. The viscosity of corn oil and polyol obtained from corn oil decreased with temperature. However, the viscosity and shear stress values of the biopolyol obtained with the modification were higher than the corn oil. This result, it is thought that corn oil is caused by the change in both the chemical bond structure and the molecular chain length. In addition, the hydroxyl number of the synthesized polyol was determined as approximately 160 mg KOH/g polyol. Polyurethane production has been carried out using biopolyol, catalysts, and initiators. The obtained polyurethane has a density of about 40 kg/m³ and a thermal conductivity value of 0.026 W/m·K. Besides, the use of filling material in polyurethane at a high rate has been weakened both the pore structure and mechanical properties. Experimental conditions have been optimized to determine an efficient and economical method for polyol synthesis and polyurethane production.

5. Acknowledgments

This work was supported by 1512 TÜBİTAK (Project No: 2170159), and Firat University Scientific Research Foundation (FÜBAP: MF.16.53).

6. Author Contribution Statement

In this study, Author 1 contributed making the design, literature review, contributed to forming the idea, the analysis of the results; Author 2 contributed to checking the spelling and checking in terms of content.

7. Ethics Committee Approval and Conflict of Interest

There is no need for an ethics committee approval in the prepared article. There is no conflict of interest with any person/institution in the prepared article.

8. References

- [1] Michel FS, Chazeau L, Cavaillé JY. "Mechanical properties of high density polyurethane foams: II effect of the filler size". *Composites Science and Technology*, 66, 2709-2718, 2006.

- [2] Liu K, Liang W, Ren F, Ren J, Wang F, Ding H. "The study on compressive mechanical properties of rigid polyurethane grout materials with different densities". *Construction and Building Materials*, 206, 270-278, 2019.
- [3] Guo A, Cho Y, Petrović ZS. "Structure and properties of halogenated and nonhalogenated soy-based polyols". *Journal of Polymer Science, Polymer Chemistry Edition*, 38, 21-39, 2000.
- [4] Mosiewicki MA, Dell'Arciprete GA, Aranguren MI, Marcovich NE. "Polyurethane foams obtained from castor oil-based polyol and filled with wood flour". *Journal of Composite Materials*, 43, 3057-3072, 2009.
- [5] Aydođmuş E, Kamışlı F. "Characterization of polyurethane produced by vegetable oil based polyols". *Academic Works in the Fields of Science, Culture and Art, Gece Kitaplığı*, 1, 51-55, 2018.
- [6] Aydođmuş E, Kamışlı F. "Modeling of rheological behavior of vegetable oils and vegetable oil-based polyols". *Academic Works in the Fields of Science, Culture and Art, Gece Kitaplığı*, 1, 57-65, 2018.
- [7] Aydođmuş E, Gür M, Kamışlı F. "The Production of Vegetable Oil-Based Polyols and Modelling of Rheological Properties". *Journal of the Turkish Chemical Society Section B: Chemical Engineering*, 1, 33-42, 2017.
- [8] Aydođmuş E, Kamışlı F. "The production of polyurethane from waste vegetable oil-based polyols and modelling of rheological properties". *Periodicals of Engineering and Natural Sciences*, 5, 81-86, 2017.
- [9] Kamışlı F, Aydođmuş E. "Generating of new types of fractal structures and developing of formula for the effective thermal conductivity of fractal porous media". *International Journal of Modern Communication Technologies and Research*, 4:1-8, 2016.
- [10] Aydođmuş E. *Synthesis of Polyols from Vegetable Oils and Characterization of the Produced Polyurethanes*. Ph.D Thesis, Fırat University, Institute of Science, Elazığ, Turkey, 2019.
- [11] Aydođmuş E, Kamışlı F. "New commercial polyurethane synthesized with biopolyol obtained from canola oil: Optimization, characterization, and thermophysical properties". *Journal of Molecular Structure*, 1256, 132495, 2022.



Production and characterization of chitosan-based polymer particles with the precipitation collection method

Çöktürme toplama metodu ile kitosan esaslı polimerik partikül üretimi ve karakterizasyonu

Hülya DEMİRTAŞ¹ , Şeyda TAŞAR^{2*} , Fatih KAYA³ , Ahmet ÖZER⁴ 

^{1,2,3,4}Department of Chemical Engineering, Faculty of Engineering, Firat University, Elazığ, Turkey.

¹hulya.demirtas2391@hotmail.com, ²sydtasar@firat.edu.tr, ³fatihkaya@firat.edu.tr, ⁴aozer@firat.edu.tr

Received: 21.01.2022
Accepted: 09.05.2022

Revision: 22.04.2022

doi: 10.5505/fujece.2022.54264
Research Article

Abstract

In this study, a chitosan-based polymer particle was produced to be used as a sorbent. Gel particle production was carried out using chitosan samples with different acetylation degrees and molecular weights. The produced particles were characterized. In the first phase of the study, chitosan samples were provided and structural analyses were performed. In the second stage, polymer particle production was carried out by the precipitation-collection method. The morphological, structural, and physicochemical properties of the produced gel particles were examined. In the last step, the sorption efficiency of the particles (distilled water, oleic acid) was investigated. As a result, it was measured that the polymer particle diameters were to be between 3.388 and 3.903 mm and the densities of the particles were to be 0.389-0.416 g/cm³. Distilled water holding capacity of the particle which was produced with an 85 % DDA chitosan sample, was calculated as 0.523 g/g_{particles}, and the oleic acid holding capacity was determined as 0.286 g/g_{particles}. These values are approximately 20 % lower than the values obtained with the 75 % DDA chitosan sample. Low molecular mass chitosan sample sorbed 0.556 g distilled water per gram particle and 0.193 g oleic acid per gram particle. These values were calculated as 0.170 g/g_{particle} and 0.381 g/g_{particle} for the particles produced using high molecular weight chitosan samples, respectively. EDX analysis performed on the selected region, it was determined that the chitosan-based polymer particle consisted of 43.58 % C, and 49.83 % O.

Keywords: Chitosan, Polymer particle, Sorption, Distilled water, Oleic acid.

Özet

Bu çalışmada, sorbent olarak kullanılmak üzere kitosan bazlı bir polimer partikülü üretilmiştir. Jel partikül üretimi, farklı asetilasyon derecelerine ve moleküler ağırlıklara sahip kitosan numuneleri kullanılarak gerçekleştirilmiştir. Üretilen partiküller karakterize edilmiştir. Çalışmanın ilk aşamasında kitosan numuneleri temin edilerek yapısal analizleri yapılmıştır. İkinci aşamada çöktürme-toplama yöntemi ile polimer partikül üretimi gerçekleştirilmiştir. Üretilen jel partiküllerinin morfolojik, yapısal ve fizikokimyasal özellikleri incelenmiştir. Son aşamada partiküllerin (distile su, oleik asit) sorpsiyon etkinliği araştırılmıştır. Sonuç olarak, polimer partikül çaplarının 3.388 ile 3.903 mm arasında ve partiküllerin yoğunluklarının 0.389-0.416 g/cm³ arasında olduğu ölçülmüştür. % 85 DDA kitosan numunesi ile üretilen partikülün distile su tutma kapasitesi 0.523 g/g_{partikül}, oleik asit tutma kapasitesi ise 0.286 g/g_{partikül} olarak belirlenmiştir. Bu değerler, % 75 DDA kitosan numunesi ile elde edilen değerlerden yaklaşık % 20 daha düşüktür. Düşük moleküler kütleli kitosan numunesi, gram parçacık başına 0.556 g damıtılmış su ve gram parçacık başına 0.193 g oleik asit emdi. Bu değerler yüksek molekül ağırlıklı kitosan numuneleri kullanılarak üretilen partiküller için sırasıyla 0.170 g/g_{partikül} ve 0.381 g/g_{partikül} olarak hesaplanmıştır. Seçilen bölge üzerinde yapılan EDX analizinde kitosan bazlı polimer partikülün % 43.58 C ve % 49.83 O içerdiği belirlendi.

Anahtar kelimeler: Kitosan, Polimer partikül, Sorpsiyon, Distile su, Oleik asit.

1. Introduction

Polymer chemistry is one of the most advanced fields of chemistry. Polymers, which were previously used only in very basic applications in industry, recently are also used in different fields (such as research in space technology, biomedicine, artificial organ construction, and controlled release of fertilizers in agriculture). The using widespread use of synthetic

*Corresponding author

polymeric products, the main raw material of which is petroleum, has brought environmental problems. It has been understood that the use of biodegradable natural polymers (which can self-degrade in nature) should become widespread instead of petroleum-based synthetic polymers that cannot self-degrade in nature. For this reason, studies have been carried out in recent years to develop natural polymeric products with biodegradable properties for areas where polymers are widely used, especially in packaging, agriculture, and medicine. Studies have focused on natural polymers such as starch, chitin, chitosan, carboxymethyl cellulose, hemicellulose, sodium alginate, xanthan gum, gelatin, etc. [1].

Chitin, which can be obtained from natural sources, is the second most common biopolymer on earth after cellulose. Chitin is obtained from the exoskeleton structures of shellfish such as crabs, lobsters and shrimps, insects, and the cell walls of fungi. Chitin is found in approximately 25 % of the shells of insects, and 15 % and 30 % in crabs and shrimps, respectively. Chitin has a stable structure and is insoluble in water, alcohol, dilute acid, and basic solutions [2]. To produce chitin from the waste shells of crustaceans, demineralization, deproteinization, and decolorization processes must be applied, respectively, to remove minerals, proteins, and pigments from the shell (Figure 1) [3-6]. While dilute sodium hydroxide solution is commonly used for the removal of proteins, dilute hydrochloric acid solution is preferred for the removal of mineral substances [7]. The decolorization treatment is ethanol, sodium hypochlorite solution, pure acetone, hydrogen peroxide, etc. carried out using chemicals. In this context, there are many studies on the production of chitin and its derivatives from waste shells and the recovery efficiency and product characterization depending on the process parameters [8-10].

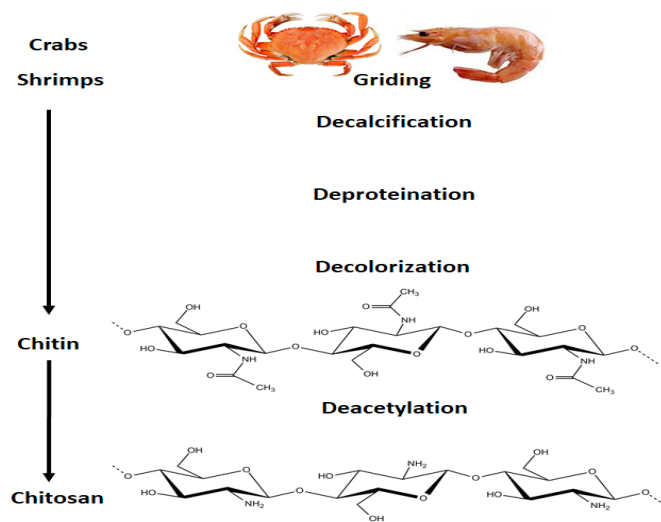


Figure 1. Chitosan production process [11]

Chitosan (poly- $[\beta\text{-(1,4)-2-amino-2-deoxy-}\beta\text{-D-glucopyranose}]$) is a linear polysaccharide. It is a deacetylated derivative of chitin and is the second most abundant biopolymer in nature after cellulose. Chitosan is a biobased macromolecule ie. polymer. It is considered to be an environmentally friendly material, due to biodegradable. In addition, chitosan renewable and hydrophilic exhibit the properties [12]. Unlike other natural polymers, chitosan macromolecules are positively charged (due to weakly basic groups) and are cationic polysaccharides. For this reason, chitosan macromolecules can easily interact with negatively charged polymers, macromolecules, and polyanions. Chitosan macromolecule can bond with many bioactive substances such as protein and lipid. And it can participate in network or matrix formation with many polymers such as negatively charged alginate. It is also compatible with important functional carbohydrates (hyaluronic acid, mucopolysaccharides) in the body. Chitosan and its derivatives have anti-cancer [13], antioxidant, anti-microbial, anticoagulant, antihypertensive, antidiabetic, antiobesity, anti-allergic, anti-inflammatory, neuroprotective, and matrix metalloproteinase inhibitory effects. They are renewable, biocompatible, biodegradable, and non-toxic compounds with biological activity [14]. Chitosan contains three functional reactive groups. They are an amino group at the C-2 position and primary and secondary hydroxyl groups at the C-3 and C-6 positions [15]. Due to the presence of functional groups in its structure, being a cationic polymer and suitable for the production of particles of different sizes, chitosan has been used especially in biomedical applications, pharmaceutical, cosmetics, and food packing sectors [16, 17].

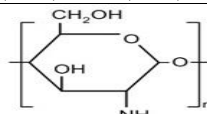
Chitosan, which had been used in limited areas such as plant growth and water treatment until the early 1990s, was described as a new generation polymer thanks to its specific properties discovered with the increase of studies on chitosan in the following years. However, the use of chitosan biopolymer in Turkey is very low compared to developed countries. Chitosan still maintains its feature of being a biopolymer whose usage area should be increased. In the last fifteen years, many studies (theses, articles) had been carried out mainly on the chitin and chitosan production methods [18-20]. Studies are concentrated in this area. However, it is emphasized that current studies should proceed in the direction of converting chitosan into products with high added value (production of chitosan-based polymeric nanoparticles and films). Especially in academic studies conducted at the international level in the last five years, chitosan has been used in the production of biomaterials, biotechnology/tissue engineering applications, and drug release applications [21-24].

Chitosan is thought that alternative sorbent. Recently, it is detailed studies are carried out to produce sorbents/ion exchangers (chitosan-based polymeric microparticles and film production) from chitosan for the removal of micropollutant, heavy metals, or dye molecules [25-29]. However, no study has been conducted to investigate the effect of chitosan DD and molecular weight on the efficiency of sorption. Therefore, in this study, firstly, chitosan samples with different deacetylation degrees and molecular weights were obtained from commercial enterprises and the samples were characterized. The chitosan particles were produced, then characterized and then sorption activity (distilled pure water, oleic acid) was investigated. There is no study in the literature examining the effect of acetylation degree and molecular weight on the physicochemical, structural, and sorption properties of the produced gel particles. It is thought that this study will contribute to the literature in this context.

2. Materials and Methods

The chemicals which were used in the chitosan-based polymeric polymer particle production step were purchased from Sigma-Aldrich (USA) and their properties were given in Table 1. All of the chemicals were high purity degrees. A total of five chitosan samples with three different molecular weights and two different deacetylation degrees (DDA) were purchased from Acros (New Jersey, USA).

Table 1. The main chemicals and their properties

Chemicals	Purity	Chemical formula
Acetic acid	≥99.85 %	CH ₃ CO ₂ H
Hydrochloric acid	ACS reagent, 37 %	HCl
Ethanol	absolute	CH ₃ CH ₂ OH
Sodium hydroxide	pellet	NaOH
Potassium hydroxide	pellet	KOH
Oleic acid (fatty acid)	ACS reagent	CH ₃ (CH ₂) ₇ CH=(CH ₂) ₇ COOH
Chitosan (Poly(D-glucosamine))	75 % and 85 % DDA Low, medium, high Mw	

2.1. Moisture content analysis

Moisture content analysis of chitosan samples was performed at 80 °C by the gravimetric method. For this purpose, the Mettler LJ16 brand moisture analyzer was used. The analysis experiments were performed using chitosan samples with a particle size of 154 µm (less than 100 mesh). All of the analysis was repeated at least three times, and the calculation results were presented by taking the average of the experiments.

2.2. Ash content analysis

The ash content analysis of chitosan samples had been performed appropriately to the ASTM-D1102 standard. The analysis experiments were performed using chitosan samples with a particle size of 154 µm (less than 100 mesh).

All of the analysis was repeated at least three times, and the calculation results were presented by taking the average of the experiments.

2.3. FTIR analysis

FTIR analysis was used to reveal the functional groups and chemical structure of chitosan samples. For this purpose, Shimadzu IR Spirit spectrophotometer was used and measurements were carried out using 45 scans in the range of 400 to 4000 cm^{-1} . A background scan was performed to prevent interference from airborne components, and then samples were scanned under the same conditions.

2.4. Determination of water and fatty acid holding capacity

Distilled water and fatty acid (oleic acid) holding (sorption) capacity of chitosan samples were determined by the gravimetric method. The experiments were carried out by the method of "The Japanese Industrial Standard K8150". For this purpose, 20 ml of distilled water or oleic acid was placed in 50 ml plastic beakers, and chitosan samples of which the initial mass was determined (W_d), were added. The samples were allowed to contact distilled water or fatty acid at 25 °C for 24 hours. At the end of the contact time, the chitosan samples were filtered and weighed, and the final weighing was recorded (W_s). The holding capacity of chitosan samples was calculated using Equation 1.

$$\text{HC} \left(\frac{\text{g}}{\text{g}_{\text{chitosan}}} \right) = \frac{(W_s - W_d)}{W_d} \quad (1)$$

2.5. Determination of the viscosity of chitosan gel solutions

1 ± 0.001 g of chitosan samples were solved in 2.5 % acetic acid solution. Before the production of polymer particles, the viscosity value of the chitosan solutions was measured using AND Vibro SV-10 brand viscometer. Thus, chitosan-based polymer particle production was made with gel solutions which is a standard viscosity range.

2.6. Production procedure of chitosan-based polymer particles

The chitosan-based polymer particle was produced by the precipitation-collection method. Deacetylation degree, molecular weight, alkali type, and alkali concentration were determined as variable parameters. The effects of these parameters on particle production and particle properties were investigated. 1 ± 0.002 gram chitosan sample was dissolved in 25 ml of acetic acid solutions (2.5 % (v/v)).

To obtain homogeneous gel solutions, an ultrasonic homogenizer of Bandelin HD 2070 was used. The homogenizer was operated with 50 % amplitude, 5 seconds spraying, and 1 second dwell time. The prepared homogeneous gel solutions were dropped with an injector to the NaOH or KOH solutions (0.5-1-5-10-20-40 g/L). The process was carried out that a maximum of 3 particles per minute was produced. The speed of the magnetic stirrer was kept at 400 rpm so that the particles did not break up. The chitosan particles were kept in the alkaline solution for one day, then filtered. It was washed with distilled water until it reached neutral pH. At the end of the washing process, the chitosan particles were taken into the 50 % distilled water-ethanol mixture.



Figure 2. A photograph of a chitosan-based polymer particle

2.7. Characterization of Chitosan Based Particles

Size determination of chitosan-based polymer particle: The diameter of the chitosan-based particle produced in a standard size by the precipitation-collection method was determined using a digital thickness gauge (caliper/micrometer). For this aim, the diameter of the particles was measured using a digital thickness gauge (caliper/micrometer) with ± 0.001 mm accuracy. Measurements were repeated for at least five particles and the measurements were averaged. Average particle diameter was used to calculate particle densities. All analyzes and tests applied for the characterization of polymer particles were carried out using the particles of standard diameter.

Distilled water and oleic acid holding capacity: Distilled water and fatty acid (oleic acid) holding (sorption) capacity of chitosan samples were determined by the gravimetric method. The experiments were carried out by the method of "The Japanese Industrial Standard K8150". The analysis details were given in the raw material analysis section.

2.8. Morphological analysis (SEM)

To reveal the surface morphology of networked particles, SEM analyses were performed using the EVO/MA10. Before SEM analysis, all particles were coated with gold.

3. Results and Discussion

3.1. Characterization of chitosan samples

In the study, firstly, chitosan samples with different deacetylation degrees and molecular weight obtained from commercial enterprises were characterized. The ash and moisture contents of the chitosan samples were given in Table 2. The moisture content of chitosan samples was found to be between 6 % and 10 %. Although the ash contents of the samples are within the expected limits, the ash content of the chitosan with 85 % deacetylation degree chitosan samples was much higher (about 4 %) compared to the other samples. The ash and moisture contents of chitosan samples were consistent with Fawzya et al (2018)'s [30] and Yuan et al (2011)'s [31] studies. In addition, according to previous studies, the molecular weight (MW) is an important parameter in chitosan properties such as crystallinity, degradation, tensile strengths, and moisture content [32-37] reported that the moisture sorption of chitosans with high MW's (600–1000 kDa) was significantly greater than those with similar DDA's but lower MW's (50–60 kDa).

The distilled water and fatty acid (oleic acid) holding capacities of chitosan samples were given in Table 3. It has been determined that the deacetylation degree of chitosan is inversely proportional to the distilled water and fatty acid holding capacity. The distilled water and oil sorption capacity decreased as the deacetylation degree increased. Besides, it was observed that the molecular weight and the distilled water holding capacity were inversely proportional, but the oil holding capacity changed in direct proportion. As the molecular weight of chitosan samples increased, the water holding capacity decreased, but the oil holding capacity increased.

All physicochemical properties of chitosan samples vary depending on the raw material source (shellfish or mushroom type), the production methodology, and the deacetylation degree of the chitosan and molecular weight of the chitosan. It is known that the solubility of chitosan samples and viscosity value of gel solution are some of the physicochemical properties. These properties generally affect occurring the particle and diameter of the particle. Thus, the viscosity of the chitosan gel solution was measured and these values were presented in Table 4. As result, it was determined that the viscosity values of the gel solution viscosity have changed a range from 1.13×10^3 to 2.83×10^3 cP. It was determined that the viscosity value of the chitosan gel solution changed inversely with the degree of deacetylation but was directly proportional to its molecular weight. Besides, considering the amount of acetic acid solution used while preparing gel solutions, it was determined that the solubility of the chitosan samples increased and the viscosity decreased as the degree of DDA increased. The experimental results obtained in this context are by the literature [38, 39].

Table 2. Ash and moisture content (wt %) of chitosan samples

Chitosan Samples	Moisture %	Ash %
75 % DDA chitosan	9.910	1.480
85 % DDA chitosan	5.670	4.400
Low molecular weight chitosan	6.000	1.750
Medium molecular weight chitosan	8.330	0.891
High molecular weight chitosan	9.000	0.255

Table 3. Distilled water and oleic acid holding capacities of chitosan samples

Chitosan Samples	Distilled water g/g _{partikül}	Oleic acid g/g _{partikül}
75 % DDA chitosan	1.274	0.911
85 % DDA chitosan	1.078	0.715
Low molecular weight chitosan	3.393	0.962
Medium molecular weight chitosan	3.072	2.384
High molecular weight chitosan	2.819	3.808

Table 4. The viscosity values of chitosan gel solutions

Chitosan Samples	cP	Acetic acid (ml)
75 % DDA chitosan	1.27x10 ³	25
85 % DDA chitosan	1.13x10 ³	9
Low molecular weight chitosan	1.56x10 ³	20
Medium molecular weight chitosan	1.76x10 ³	25
High molecular weight chitosan	2.83x10 ³	30

FTIR spectra of the chitosan sample are provided in Figure 1. Peaks at 3000-3500 cm⁻¹ indicate the presence of the -NH₂ (νNH) and the -OH. It is known that these two peaks coincided in this region. The apparent peak observed in the 2850-2720 cm⁻¹ region is due to the symmetric or asymmetric -CH₂ stretching vibration attributed to the pyranose ring (νC-H). Besides, it was observed that the other main peaks; at 1640 cm⁻¹ are due to expressing the vibration of the -C=O in the acetamide group (amide I band); at 1590 is due to -NH₂ bending vibration in the amino group (δNH); at 1420 and 1320 cm⁻¹ are due to vibrations of -CH in the ring, at 1250 cm⁻¹ is due to C-O group, at 1152 cm⁻¹ is due to -C-O-C in a glycosidic linkage, at 1020 cm⁻¹ is due to C-O stretching in acetamide (νC-O), and at 899 cm⁻¹ is due to corresponds to saccharide structure. The spectrum obtained agreed with the previous studies [40-42].

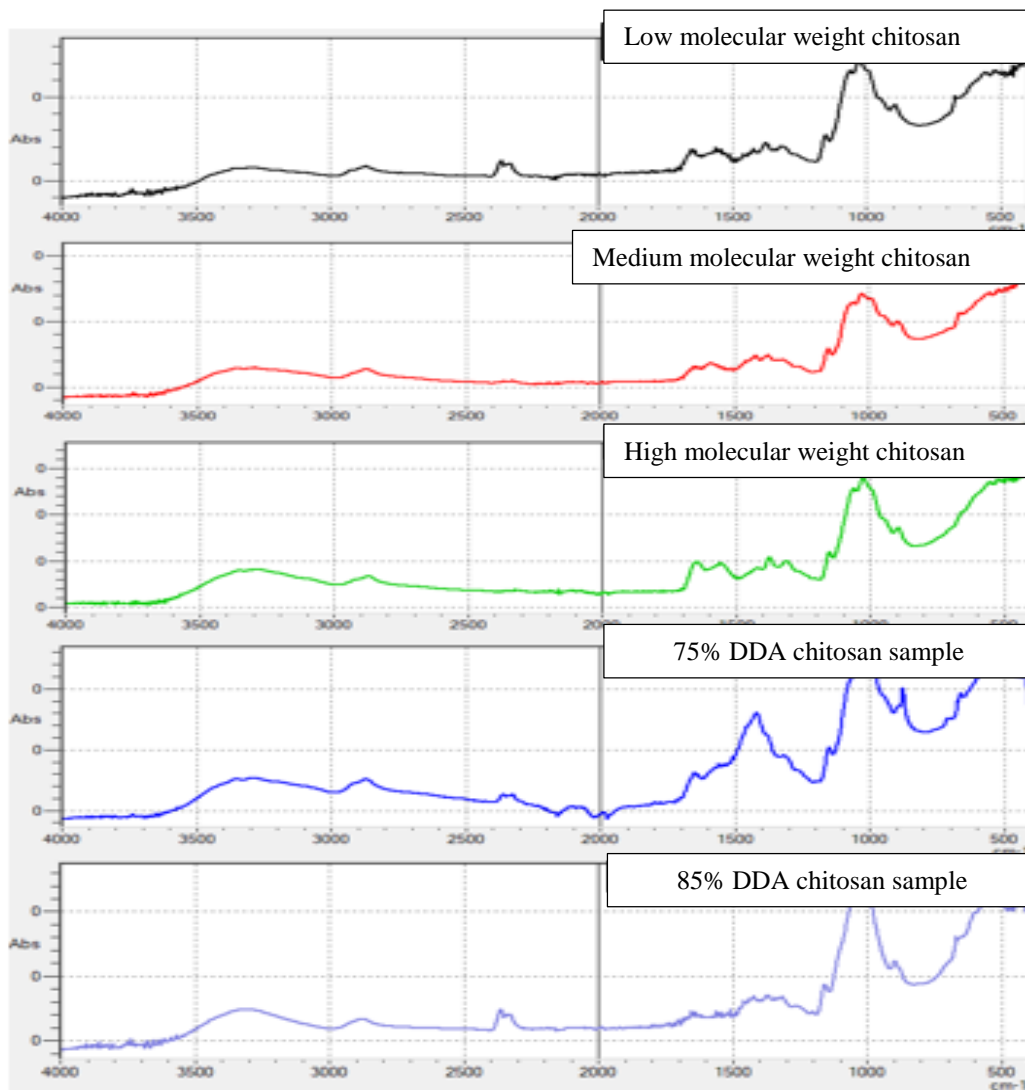


Figure 3. FTIR spectrum of chitosan samples

3.2. Characterization of chitosan particles

3.2.1. The average particle size, particle density, and particle weight

The prepared in different circumstances chitosan particle's physical properties (particle's diameter, density of the particles, particle mass) are presented in Table 5. The mass of the particles has changed the range from 0.036 to 0.047 g. The particle diameters were measured between 3.388-3.903 mm. Depending on these parameters, the densities of the particles were calculated as 0.389-0.416 g/cm³.

Besides, it was observed that there is a nonlinear increase in the diameter and mass of the particles as the alkali concentration increased. In addition, the particles which were prepared using KOH solution as an alkaline medium, have a relatively higher diameter and mass compared to the particles prepared using NaOH solution. And their physical strength was higher than the particles prepared with NaOH.

Table 5. Sizes, masses, and densities of chitosan particles

Alkaline	Alkaline con.	Particle weight (g)	Particle diameter (mm)	Particle density (g/cm ³)
NaOH	1 g/L	0.036	3.388	0.400
	5 g/L	0.037	3.470	0.391
	10 g/L	0.038	3.495	0.396
	20 g/L	0.042	3.588	0.416
	40 g/L	0.043	3.598	0.423
KOH	1 g/L	0.036	3.388	0.400
	5 g/L	0.038	3.470	0.402
	10 g/L	0.044	3.797	0.389
	20 g/L	0.047	3.870	0.400
	40 g/L	0.047	3.903	0.393

3.2.2. Distilled water and fatty acid holding capacities of chitosan particles

Distilled water and fatty acid (oleic acid) holding capacities of chitosan particles are presented in Table 6. It was determined that the deacetylation degree was inversely proportional to the distilled water and fatty acid holding capacity. As the deacetylation degree increased, the sorption capacity decreased. Distilled water holding capacity of the particle which was produced with an 85 % DDA chitosan sample, was calculated as 0.523 g/g particles, and the oil holding capacity was calculated as 0.286 g/g particles. These values are approximately 20 % lower than the values obtained with the 75 % DDA chitosan sample.

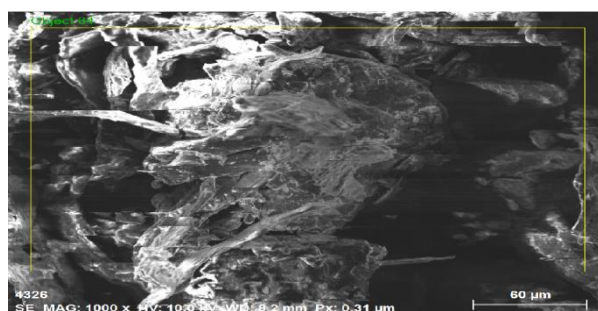
It was determined that as the molecular weight of chitosan samples increased, their oleic acid holding capacity increased, and distilled water holding capacity decreased. Low molecular mass chitosan sample sorbed 0.556 g distilled water per gram particle and 0.193 g oleic acid per gram particle. These values were calculated as 0.170 g/g_{particle} and 0.381 g/g_{particle} for the particles produced using high molecular weight chitosan samples, respectively. The results are in agreement with the data obtained from the chitosan samples given in Table 3.

Table 6. Water and fatty acid (oleic acid) sorption capacities of chitosan particles

Chitosan polymer particle	Distilled water (g/g _{partikül})	Oleic acid(g/g _{partikül})
75 % DDA chitosan-based particle	0.523	0.286
85 % DDA chitosan-based particle	0.647	0.381
Low molecular weight chitosan-based particle	0.556	0.193
Medium molecular weight chitosan-based particle	0.298	0.222
High molecular weight chitosan-based particle	0.170	0.381

3.2.3. SEM analysis of chitosan and chitosan-based polymer particle

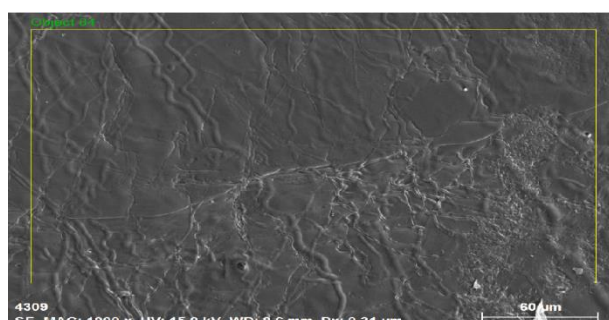
The SEM images of the 75 % DDA chitosan sample and the chitosan particle which was produced using the 75 % DDA chitosan sample are given in Figure 4 and Figure 5, respectively. According to the 1000 times magnified image, it is understood that chitosan has a layered structure in the macro sense. However, in some parts of these layer fragments, a whitish sheen was noted. The presence of calcium (Ca) was detected in the structure as a result of the EDX analysis performed in a region that will include these whitish sheen. According to the spectrum obtained from the EDX analysis performed on the selected region in Figure 4, it was determined that the chitosan sample consisted of 37.45 % C, 53.21 % O, and 8.06 % Ca. According to Figure 5, it is understood that chitosan-based polymer particle has a homogenous, nonporous, and smooth structure in the macro sense. EDX analysis performed on the selected region in Figure 5, it was determined that the chitosan-based polymer particle consisted of 43.58 % C, and 49.83 % O.



Spectrum: Object 84

El	AN	Series	Net un.	C norm.	C Atom.	C Error (1 Sigma)
			[wt.%]	[wt.%]	[at.%]	[wt.%]
O	8	K-series	1980	53.21	53.21	49.74
C	6	K-series	2164	37.45	37.45	46.63
Ca	20	K-series	317	8.06	8.06	3.01
P	15	K-series	131	1.27	1.27	0.62
Total:			100.00	100.00	100.00	

Figure 4. SEM image of 75% DDA chitosan samples



Spectrum: Object 84

El	AN	Series	Net un.	C norm.	C Atom.	C Error (1 Sigma)
			[wt.%]	[wt.%]	[at.%]	[wt.%]
O	8	K-series	2166	49.83	49.83	43.18
C	6	K-series	3509	43.58	43.58	50.30
N	7	K-series	118	6.59	6.59	6.52
Total:			100.00	100.00	100.00	

Figure 5. SEM image of chitosan particle produced with 75 % DDA chitosan sample

4. Conclusion

In this study, chitosan particles were produced by using chitosan samples with different deacetylation degrees and molecular weights obtained from commercial enterprises to be evaluated as sorbent.

- The moisture content of the chitosan samples was high and the ash content was within the expected limits, but the ash content of the chitosan samples with 85 % deacetylation degree was quite higher than the other samples.
- The water and oleic acid holding capacity were inversely proportional to the deacetylation degree, and as the deacetylation degree increased, the water and oleic acid sorption capacity decreased.
- The viscosity value of chitosan gel solutions changed inversely with the deacetylation degree of chitosan and was directly proportional to the molecular weight.
- It was determined that all chitosan samples show similar characteristic peaks in their FTIR spectra, mainly containing stretching vibrations and bands of $-NH_2$, $-C=O$, $-OH$, and $-C-O-C$.
- It was measured that the polymer particle diameters were to be between 3.388 and 3.903 mm and the densities of the particles were to be 0.389-0.416 g/cm³. The diameter and weight of the particles increased as the alkali concentration increased.
- The particles prepared using the KOH solution have a relatively higher diameter and mass than the particles prepared using the NaOH solution.
- The physical strength of the particles prepared by using KOH solution was higher than the particles prepared with NaOH.
- The degree of deacetylation is inversely proportional to the distilled water and fatty acid holding capacity, and as the degree of deacetylation increases, the sorption capacity decreases. Distilled water holding capacity of the particle which was produced with an 85 % DDA chitosan sample, was calculated as 0.523 g/g_{particles}, and the oleic acid holding capacity was determined as 0.286 g/g_{particles}. These values are approximately 20 % lower than the values obtained with the 75 % DDA chitosan sample. Low molecular mass chitosan sample sorbed 0.556 g distilled water per gram particle and 0.193 g oleic acid per gram particle. These values were calculated as 0.170 g/g_{particle} and 0.381 g/g_{particle} for the particles produced using high molecular weight chitosan samples, respectively.

- According to the morphological analysis, chitosan has a layered structure. The chitosan-based polymer particle has a homogenous, nonporous, and smooth structure.
- EDX analysis performed on the selected region, it was determined that the chitosan-based polymer particle consisted of 43.58 % C, and 49.83 % O. It was obtained that the chitosan sample consisted of 37.45 % C, 53.21 % O, and 8.06 % Ca.

5. Author Contribution Statement

In the study, Author 1 experimental studies has carried out; Author 2 planned the process, interpreted the experimental results, and writing-original draft; Author 3 methodology, interpreted the experimental results, and writing-original draft; Author 4 investigation, interpreted the experimental results, and writing-original editing.

6. Ethics Committee Approval and Conflict of Interest

There is no need for any an ethics committee approval in the prepared article.

7. References

- [1] Sharma S, Sudhakara P, Singh J, Ilyas RA, Asyraf MRM, Razman MR. "Critical review of biodegradable and bioactive polymer composites for bone tissue engineering and drug delivery applications". *Polymers*, 13(16), 2623, 2021.
- [2] Fernandez-Kim SO. Physicochemical and Functional Properties of Crawfish Chitosan as Affected by Different Processing Protocols. MS dissertation, Louisiana State University, Baton Rouge, L.A., 2004.
- [3] Tajik H, Moradi M, Rohani SMR, Erfani AM, Jalali FSS. "Preparation of chitosan from brine shrimp (*artemia urmiana*) cyst shells and effects of different chemical processing sequences on the physicochemical and functional properties of the product". *Molecules*, 13, 1263-1274, 2008.
- [4] Peker İ, Oktar F, Eroğlu M, Morkoç E. "Kerevit kabuklarından kitosan üretilmesi ve kesilmiş sütün suyundan laktoz izolasyonu işleminde kullanılması". TÜBİTAK MAG Project, Project number: 104M017, 88, 2006.
- [5] Rinaudo, M. "Chitin and chitosan: properties and applications". *Progress in Polymer Science*, 31, 603-632, 2006.
- [6] Nemtsev SV, Gamzazade AI, Rogozhin SV, Bykova VM, Bykov VP. "Deacetylation of chitin under homogeneous conditions". *Applied Biochemistry and Microbiology*, 38 (6), 521-526, 2002.
- [7] Paulino AT, Simionato JI, Garcia JC, Nozaki J. "Characterization of chitosan and chitin produced from silkworm crysalides". *Carbohydrate Polymers*, 64, 98-103, 2006.
- [8] Hajji S, Younes I, Ghorbel-Bellaaj O, Hajji R, Rinaudo M, Nasri M, Jellouli K. "Structural differences between chitin and chitosan extracted from three different marine sources". *International Journal of Biological Macromolecules*, 65, 298-306, 2014.
- [9] Kaur S, Dhillon GS. "The versatile biopolymer chitosan: potential sources, evaluation of extraction methods and applications". *Critical Reviews in Microbiology*, 40, 155-175, 2014.
- [10] Kurita K. "Chitin and chitosan: Functional biopolymers from marine crustaceans". *Marine Biotechnology*, 8, 203-226, 2006.
- [11] GlycoPedia. "Extraction of Chitin & Preparation of Chitosan" <https://www.glycopedia.eu/e-chapters/from-chitin-to-chitosan/article/extraction-of-chitin-preparation-of-chitosan> (21.01.2022).
- [12] Du J, Tan E, Kim HJ, Zhang A, Bhattacharya R, Yarema KJ, "Comparative evaluation of chitosan, cellulose acetate, and polyethersulfonenanofiber scaffolds for neural differentiation". *Carbohydrate Polymers*, 99,483-490, 2014.
- [13] Salah R, Michaud P, Mati F, Harrat Z, Lounici H, Abdi N, Drouiche N, Mameri N. "Anticancer activity of chemically prepared shrimp low molecular weight chitin evaluation with the human monocyte leukaemia cell line". THP-1. *International Journal of Biological Macromolecules*, 52, 333-339, 2013.
- [14] El-Aidie SAM. "A review on chitosan: ecofriendly multiple potential applications in the food industry ". *Int J Adv Life Sci Res.*, 1 (1), 1-14, 2018.





- [15] Youssef AM, Abou-Yousef H, El-Sayed SM, Kamel S. “Mechanical and antibacterial properties of novel high-performance chitosan / nanocomposite films”. *International Journal of Biological Macromolecules*, 76, 25-32, 2015.
- [16] Montazer M, Afjeh G, “Simultaneous x-linking and antimicrobial finishing of cotton fabric”. *Journal of Applied Polymer Science*, 103,178-185, 2007.
- [17] Demir A, Seventekin N. “Chitin, chitosan and general uses”. *Textile Technologies Electronic Journal* , 92-103, 2009.
- [18] Koçer İ. Chitosan is Obtained by Various Methods and Characterization , M.Sc., Hacettepe University, Institute of Science and Technology in Ankara, Turkey, 2015.
- [19] Tokatlı K. Shrimp Optimization of Production Conditions of Chitosan and Chitosan from Waste Edible Films Obtained Effects of Shelf Life Cherry Veneer, Gaziosmanpasa University, Science Institutes bases in Tokat, Turkey, 2016.
- [20] Çarıkçı TD. Shellfish Ultrasonic Reactor Waste Chitosan Production/Production of chitosan from shellfish waste in an ultrasonic reactor, Bilecik Sheikh Edebali University, Institute of Science, Istanbul, Turkey, 2015.
- [21] Boamah PO, Huang Y, Zhang Q, Wu J. “Sorption of heavy metal ions onto carboxylate chi tosan derivatives-a mini-review”. *Ecotoxicol. Environ.*, 116, 113–120, 2015.
- [22] Demarchi C, Debrassi A, Dluż ewski P, Scapinello J. “Adsorption of the dye remazol red 198 (rr198) by o-carboxymethylchitosan-N-lauryl /Fe₂O₃ magnetic nanoparticles”. *Arabian Journal of Chem.*, 12 (8), 3444-3453, 2015.
- [23] Kyzas GZ Kostoglou M, Lazaridis NK. “Relating interactions of dye molecules with chitosan to adsorption kinetic data”. *Langmuir Article*, 26, 9617-9626, 2010.
- [24] Soltani RDC, Khataee AR, Safari M, Joo SW. “Preparation of bio-silica/chitosan nanocomposite for adsorption of a textile dye in aqueous solutions”. *International Biodeterioration & Biodegradation*, 85, 383-391, 2013.
- [25] Boamah PO, Huang Y, Zhang Q, Wu J. “Sorption of heavy metal ions onto carboxylate chitosan derivatives-a mini-review”. *Ecotoxicology and Environmental Safety*, 116: 113–120, 2015.
- [26] Bozorgpour F, Ramandi HF, Jafari P, Samadi S, Yazd SS, Aliabadi M. “Removal of nitrate and phosphate using chitosan/Al₂O₃/Fe₃O₄ composite nanofbrous adsorbent: Comparison with chitosan/Al₂O₃/Fe₃O₄ beads”. *Int J Biol Macromol*, 93, 557–565, 2016.
- [27] Chethan PD, Vishalakshi B. “Synthesis of ethylenediamine modified chitosan microspheres for removal of divalent and hexavalent ions”. *Int J Biol Macromol*, 75:179–185, 2015.
- [28] Demarchi C, Debrassi A, Dluż ewski P, Scapinello J. “Adsorption of the dye remazol red 198 (rr198) by o-carboxymethylchitosan-N-lauryl / Fe₂O₃ magnetic nanomicroparticles”. *Arabian Journal of Chemistry*, 12 (8), 3444-3453, 2015.
- [29] Filipkowska U, Józwiak T. “Application of chemically-cross-linked chitosan for the removal of reactive black 5 and reactive yellow 84 dyes from aqueous solutions”. *Journal of Polymer Engineering*, 33, 8, 735-747, 2013.
- [30] Fawzya YN, Rahmawati A, Patantis G, “Physicochemical properties of chitoooligosaccharide prepared by using chitosanase from *Stenotrophomonas maltophilia* KPU 2123”. *Journal of Earth and Environmental Sciences*, 139 012045, 2018.
- [31] Yuan Y, Chesnutt BM, Haggard WO, Bumgardner JD. “Deacetylation of chitosan: Material characterization and in vitro evaluation via albumin adsorption and Pre-osteoblastic cell cultures”. *Materials*, 4, 1399-1416, 2011.
- [32] Ogawa K, Yui T. “Structure and function of chitosan. 3. Crystallinity of partially N-acetylated chitosans”. *Biosci. Biotech. Bioch.*, 57, 1466-1469, 1993.
- [33] Zhang Z.T, Chen DH, Chen L. “Preparation of two different serials of chitosan”. *J. Dong Hua Univ. (Eng. Ed.)* 19, 36-39, 2002.
- [34] Knaul JZ, Kasai MR, Bui VT, Creber KAM. “Characterization of deacetylated chitosan and chitosan molecular weight review”. *Can. J. Chem.*, 76, 1699-1706, 1998.
- [35] Xu Y, Du Y. “Effect of molecular structure of chitosan on protein delivery properties of chitosan nanoparticles”. *Int. J. Pharm.*, 250, 215-226, 2003.
- [36] Zhang H, Neau SH. “In vitro degradation of chitosan by a commercial enzyme preparation: effect of molecular weight and degree of deacetylation”. *Biomaterials*, 22, 1653-1658, 2001.
- [37] Nunthanid J, Puttipatkhachorn S, Yamamoto K, Peck G.E. “Physical properties and molecular behavior of chitosan films”. *Drug Dev. Ind. Pharm.*, 27, 143-157, 2001.

- [38] Shijie (Gabriel) K, Linda M, Michael P, Mucalo R. “Chitosan: A review of sources and preparation methods”. *International Journal of Biological Macromolecules*, 169, 85—94, 2021.
- [39] Younes I, Rinaudo M. “Chitin and chitosan preparation from marine sources, Structure, properties and applications”. *Marine Drugs*, 13 (3), 1133—1174, 2015.
- [40] Mitra T, Sailakshmi G, Gnanamani A, Mandal AB. “Studies on cross-linking of succinic acid with chitosan/collagen”. *Mater. Res.*, 16, 755-765, 2013.
- [41] Anirudhan TS, Rijith S, “Glutaraldehyde cross-linked epoxyaminated chitosan as an adsorbent for the removal and recovery of copper (II) from aqueous media”. *Colloids Surf. A Physicochem. Eng. Asp.*, 351, 52—59, 2009.
- [42] Sowmya A, Meenakshi S. “A novel quaternized chitosan – melamine – glutaraldehyde resin for the removal of nitrate and phosphate anions”. *Int. J. Biol. Macromol*, 64, 224-232, 2014.



A novel design for concrete culverts absorbing explosive energy from homemade explosives

Ev yapımı patlayıcılardan oluşan patlayıcı enerjisini sönmüleyen beton büzler için yeni bir tasarım

Sedat SAVAŞ¹ , Dursun BAKIR^{2*} , Muharrem BAŞPINAR³ , Mehmet ÜLKER⁴ 

^{1,2,3}Department of Civil Engineering, Faculty of Engineering, Firat University, Elazig, Turkey.

⁴Department of Civil Engineering, Faculty of Engineering, Turgut Ozal University, Malatya, Turkey.

¹ssavas@firat.edu.tr, ²dbakir@firat.edu.tr, ³muharrem_baspinar@hotmail.com, ⁴mulker44@gmail.com

Received: 28.03.2022

Revision: 07.05.2022

doi: 10.5505/fujece.2022.66376

Accepted: 12.05.2022

Research Article

Abstract

With the increasing number of terrorist attacks for the last 40 years, terrorist organizations have devised various attack tactics. One of these tactics is to attack by placing homemade explosives inside culverts that are originally constructed for draining water within road infrastructure. The aim of this study is to enable the absorption of the explosive blast in concrete culverts in face of homemade explosives. For this purpose, concrete culverts that were within three road embankments and road infrastructures were built by projects that were devised according to the American Association of State Highway and Transportation Officials Standards. The experiment was carried out in three stages. In the first one of these culverts, a standard road was built. In the second and third culverts, a system that enabled the installation of secondary culverts above and below primary culverts was devised. In conclusion, it was revealed that the methods developed in the study could enable the absorption of the explosive energy of homemade explosives by 60%-80%.

Keywords: Explosion load, Absorption of explosive energy, Concrete culvert, Homemade explosive, Road design against terrorist attacks.

Özet

Son 40 yılda terör saldırılarının artmasıyla birlikte terör örgütleri çeşitli saldırı taktikleri geliştirmiştir. Bu taktiklerden biri, yol altyapısındaki suyu tahliye etmek için yapılmış olan büzlerin içine ev yapımı patlayıcılar yerleştirilerek saldırı yapmaktır. Bu çalışmanın amacı, ev yapımı patlayıcılar karşısında beton büzlerdeki patlama enerjisinin sönmülmesini sağlamaktır. Bu amaçla, Amerikan Devlet Karayolları ve Ulaştırma Yetkilileri Birliği Standartlarına göre tasarlanan projelerle üç yol dolgusu ve yol altyapısı içerisinde yer alan beton büzler hazırlanmıştır. Bu büzlerden ilkinde standart bir yol yapılmıştır. İkinci ve üçüncü büzlerde ise birincil büzlerin üstüne ve altına ikincil büzlerin kurulmasını sağlayan bir sistem geliştirilmiştir. Sonuç olarak, çalışmada geliştirilen yöntemlerin ev yapımı patlayıcıların patlama enerjisinin %60-80 oranında emilmesini sağlayabildiği ortaya konulmuştur.

Anahtar kelimeler: Patlama yükü, Patlayıcı enerjisinin emilimi, Beton büz, Ev yapımı patlayıcı, Terrorist saldırılara karşı yol dizaynı.

1. Introduction

The aims of terrorist organizations are always political. These aims can cover changing economic systems and social policies, or spreading a socioeconomic or religious ideology. Common physical damage and destruction to physical properties are primary goals [1]. As events related to terrorist attacks are increased and various types of attacks for smarter operations are developed, transportation systems have been chosen as ideal targets for terrorist organizations [2]. Over transportation systems and related infrastructures, terrorist threats for various destinations, including shopping malls, hotels, and restaurants, have been especially increased for the last 25 years [3].

In Turkey, it has been observed that terrorist organizations have been choosing homemade explosives (HMEs) since 2015. In 2016, when the explosions were at the highest frequency, landmines were used 11 times while HMEs were used 93

*Corresponding author

times. Because HMEs are prepared conveniently, they have become the most commonly adopted method of asymmetrical war today. In most cases, those explosives are manufactured in hidden laboratories. The raw materials of these types of explosives are conveniently obtained, which include urea nitrate, triacetone triperoxide (TATP), and hexamethylene triperoxide diamine (HMTD) [4]. Figure 1 demonstrates HMEs that were planted by terrorist organizations and discovered by law enforcement agencies.



Figure 1. Images of HMEs planted and hidden in culverts [5–7]



Figure 2. Images of damages resulting from explosions [8,9]

In the literature, a study conducted by M. Kristoffersen et al. investigated the explosions of C4 explosives inside a concrete pipe culvert with a 2 m diameter [10]. Furthermore, P. Bonalumi et al. examined the pressure that was created by explosions within culverts by using 10 g and 12 g of explosives [11]. Olarewaju et al. In their study, 50kg TNT explosive on concrete pipes was modeled numerically, taking into account the ground environment, and its static and dynamic effects were investigated [12]. Olarewaju et al. In another study they have done, various explosions have been applied numerically in the analysis, design and simulation of underground structures, in a way to withstand the bursting effect of concrete pipes. Explosion inside the concrete pipe, blasting at the standoff distance and open trench explosions were investigated. Considering the concrete and soil parameters with different Young modules, pipe designs were also studied. The effects of thickness variation were also investigated [13]. Mohsen Parviz et al. Parametric studies were carried out on concrete pipes placed on two different soil types under blast loading. The effects of different parameters such as water, air, soil, pipe and TNT explosive properties were investigated. Arbitrary Lagrange-Eulerian (ALE) method is used in LS-DYNA software. The results of the study revealed that a higher soil density causes a higher pressure and stress transfer on a pipe. Explosion under a lower soil density results in less damage to the pipe [14]. Qichen Tang et al. A field experimental study of the dynamic response properties of buried pipelines under surface burst load was carried out to investigate the effect of blast load on pipelines located underground. The ground surface peak particle velocity (PPV) above the pipeline was analyzed under blast load with various explosive charges and different detonation distances. In addition, the PPV and peak particle stress (PPS) distribution properties of pipelines under surface bursting were investigated. After the blasts were made, it was revealed that there is a linear relationship between the PPV of the ground surface above the pipeline and the PPV of the buried pipeline. According to the soil functions of the blastings applied in the experiment site, in order to protect the pipeline in surface blasts, it was buried at a depth of 2 m, just above the pipeline. It is emphasized that the PPV of the ground surface should be less than 71.36 cm [15].

In this study, as can be seen in Figures 1 and 2, it was aimed to reduce the potential damages that result from the explosion of HMEs placed inside culverts, which are convenient in terms of costs and camouflages. For this purpose, three techniques

were developed. In the first two construction techniques, it is aimed to discharge the explosive energy by building a secondary culvert that is in contact with the primary culvert in a way that is hidden under the road infrastructure. In the third construction technique, it is aimed to install geotextile membranes between each 20-cm ground backfill layers above the culverts during the construction of the road infrastructure. The goal of this technique is to dissipate the explosive load through a wider area on the road surface by preventing the explosion, which was demonstrated in Figure 2, to burst from a certain area of the surface. The ultimate aim of this technique is to dissipate the explosive load throughout a larger area and reduce its impact by the same ratio.

In each test, 50 kg of ammonium nitrate and fuel oil (ANFO) and 3 kg of trinitrotoluene (TNT) with electric detonators, which were manufactured by adopting the manufacturing techniques of terrorist organizations, were placed within culverts and after the necessary compactions were conducted, the explosives were detonated. Each explosion was recorded by three stationary cameras and one camera drone.

The footage obtained from the cameras in the tests was scaled by the image processing technique and the distances that materials traveled due to dislocation from the road by the explosion were measured. The velocity of detonation (VoD) device was used in the measurements of the explosions. The explosions were conducted under the supervision and observation of law enforcement agencies. Additionally, the explosions were conducted by two demolition experts, who were certified in the matter of explosions by legal authorities.

2. Methodology

The locations that are convenient for planting and camouflaging explosives on roads and chosen by terrorist organizations are concrete culverts, which are used in road infrastructures and were demonstrated in Figure 3. Reinforced concrete culverts are commonly used in infrastructures of railways and highways to enable the transfer of water, vehicles of pedestrians. Common types of culverts include slab culverts, arch culverts, pipe culverts, and box culverts [16]. In terms of the interaction between the culvert structure and the soil materials that cover the culvert, the difference in stiffness of the material of the culvert and the surrounding soil is of great importance. This is because a concrete culvert mainly carries the external load on it by its strength [17].

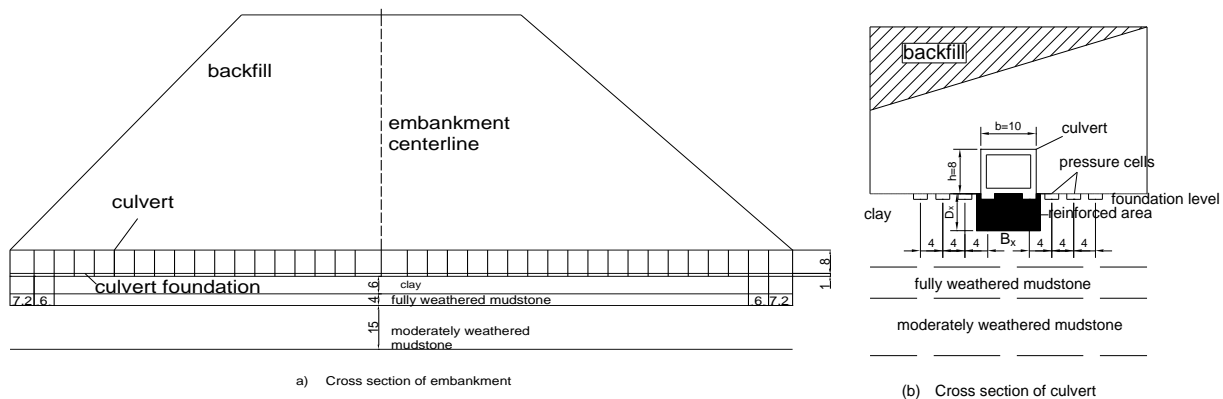


Figure 3. Field layout of the culvert, cross-sections of embankment and culvert

In this study, the pipe concrete type of culverts was used. These types of culverts are manufactured by fabrication and provide convenient transfer and installation as infrastructure components (Figure 4).



Figure 4. Concrete pipe culverts

2.1. Homemade Explosives

In recent years, urea nitrate has been frequently used in manufacturing HME by terrorist organizations due to its convenience and easy accessibility. In most cases, these explosives are manufactured in hidden laboratories. The main component of these explosives is urea nitrate, triacetone triperoxide (TATP), and hexamethylene triperoxide diamine (HMTD) (Figure 5).

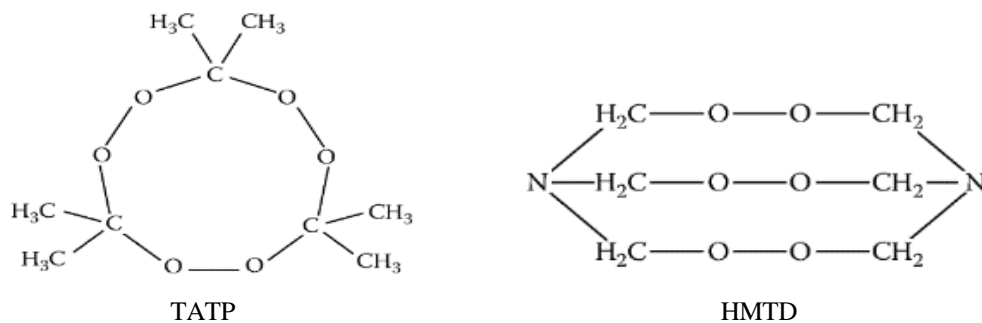


Figure 5. Structural formulae of TATP and HMTD, respectively [18]

Urea nitrate is manufactured by using nitric acid and urea. Urea is a commonly used fertilizer and it is easily accessible. Urea nitrate has never been used as a commercial explosive due to its abrasive qualities. TATP is a product of the combination of hydrogen peroxide and acetone. In recent years, these materials have become popular choices of terrorist organizations worldwide. Mercury fulminate has been a standard main charge in detonators. Although it has not been significantly used commercially, it is regarded as a serious explosive material. The precursors of the explosives in question are commercial products.

2.2. Experimental tests

The study was conducted in a quarry, which was located in the Pütürge District of the City of Malatya in Turkey. The quarry had an altitude of 1200 meters. For the video recordings, 3 stationary cameras and 1 camera drone were used.



Figure 6. Image of the field used for explosions

In the tests, HMEs that were planted inside four culverts under road infrastructures were detonated. For the preparation of these setups, one excavator, two dumper trucks, one loader, one ground compaction vibratory roller were used while one mobile winch and one sprinkler were used for the installation of the culverts (Figure 6). On highways, culverts with various sizes and diameters are used under backfills. Readily manufactured concrete culverts are manufactured in culvert worksites that are organized in suitable places for projects. In the manufacturing process, the culverts are built in steel molds that are manufactured in certain sizes (Figure 7).



Figure 7. The installation process of the culverts

2.3. Planting process of HMEs

The method that was adopted while planting the explosives within culverts was implemented according to the terrorist practices that were reported by the media and law enforcement agencies. In Figure 8, the schematic for planting and compacting the explosives was presented. In terrorist activities, the steps of planting explosives include an initial step of compaction to increase the explosive energy of the culvert that hosts the explosive. Rocks or sandbags are used for these compaction practices. Then, the material, which is referred to as fertilizers in the market, and diesel are mixed and compacted in the 17-kg tin or water cans, or 12-kg gas cylinders to be placed in culverts. In the next step, dynamites and detonation cords are placed in the setup as detonators attached to a cable system that extends to a certain distance outside of the culvert. The amounts of explosives used are given in Table 1. Then, the planted explosive is compacted once more with rocks or sandbags and the setup is completed. The explosion is triggered by a remote detonator or extended cables from a faraway place from the culvert during the transit of a vehicle from the road. The process for planting the explosive setup is completed quickly, which prevents third parties from obtaining information about the explosive. This also prevents complete compaction. In this study, we followed the exact steps above one by one while planting the explosive setups.

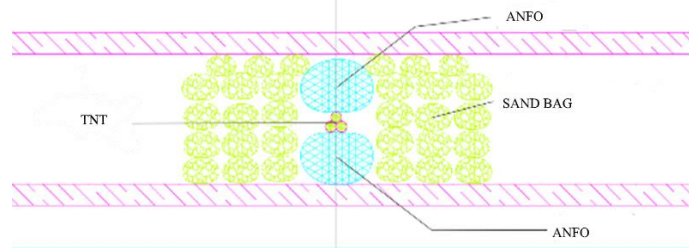


Figure 8. Schematic image of the HME setup

Table 1. Contents of the HMEs in the study

TNT	1.50 kg
ANFO	2 x 25 kg
Electrical Aluminum Capsule	1 set
Electric Cable	250 meters

2.4. The first test setup

In the explosive setup, crushed rock materials within nylon sacks, each weighing 30 kg of rocks with 0-14 mm diameters, were prepared for 21 sacks. 11 sacks were placed before planting the HME while 10 sacks were placed after planting the HME for compaction. In Figure 9, the preparations for planting the explosive setup were presented.



Figure 9. The preparation process for planting the first test setup

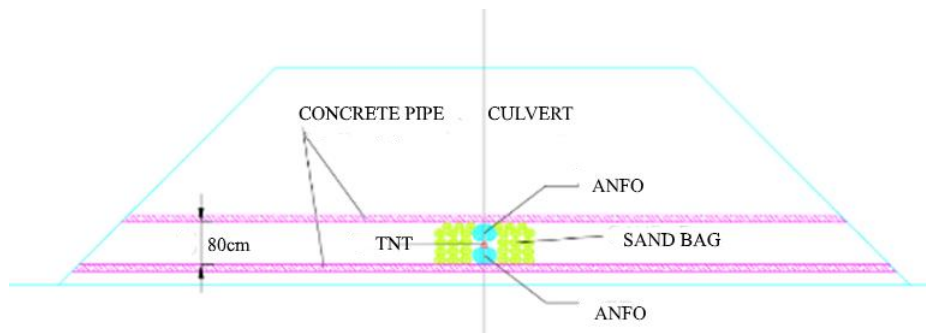


Figure 10. Cross-section image of the first test setup

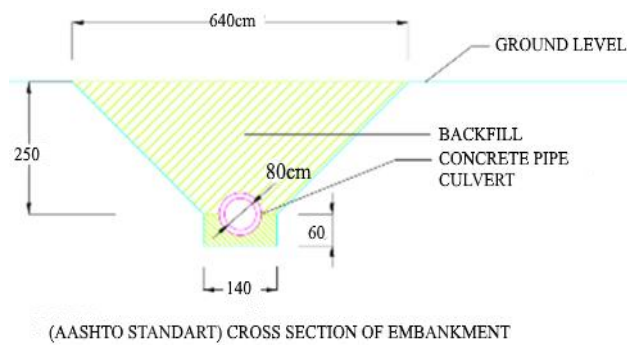


Figure 11. Cross-section image of the standard road

The schematic presentations of the HME setups in Figures 10 and 11 are in the middle of the road's axis. To reduce the impact of the explosive blast, sandbags were placed on the sides of the HME setup. The goal of placing sandbags on the sides of the explosive setup is to ensure compaction and redirect the explosive blast over the road. In other words, the goal is to prevent the explosive blast from discharging through the sides of the culvert. In Figure 12, the images of the explosions and the crater holes that were formed after the explosions were presented. The wave speed and sound measurement data of this explosion were presented in Table 2.

Table 2. Data summary of System 1

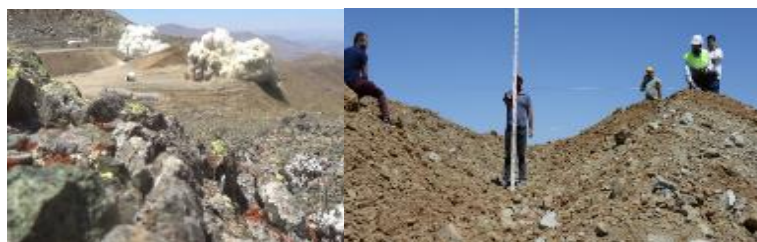
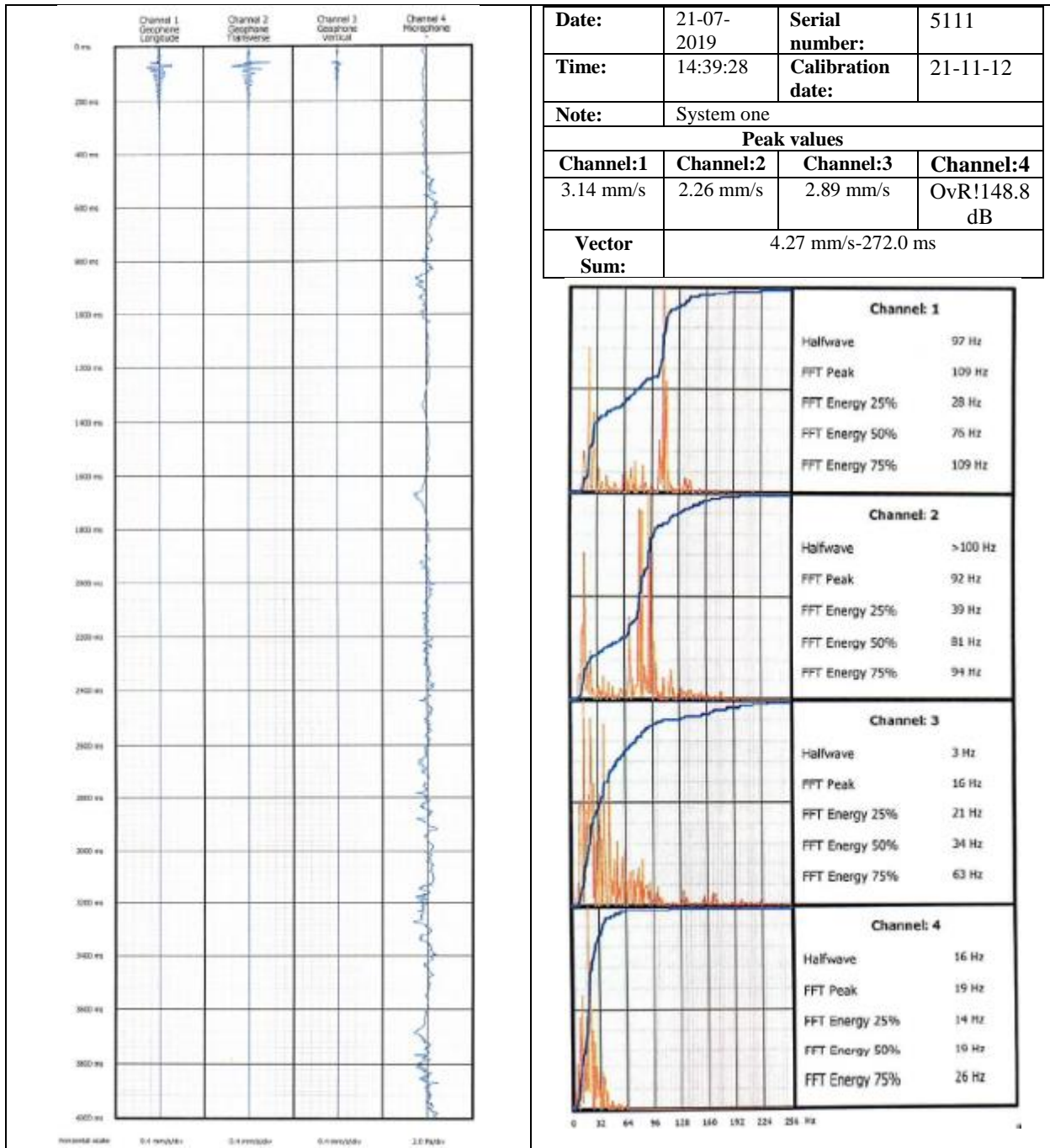


Figure 12. The explosion of the first step and the images of the aftermath

2.7. The third and fourth test setups

The explosive setup was prepared in a way to ensure a single explosion by combining two explosive setups. The third setup was prepared in a way that an 80-cm culvert (5 embedded pieces of culverts, 2 m each) was placed below and a 60-cm culvert (7 embedded pieces of culverts, 1.5 m each) was placed above. The fourth setup was prepared in a way that an 80-cm culvert (5 embedded pieces of culverts, 2 m each) was placed above and a 60-cm culvert (7 embedded pieces of culverts, 1.5 m each) was placed below. The third and fourth explosive setups were detonated by the demolition expert. The wave speed and sound measurement data of this explosion were presented in Table 3 and Table 4.

Table 3. Data summary of System 3

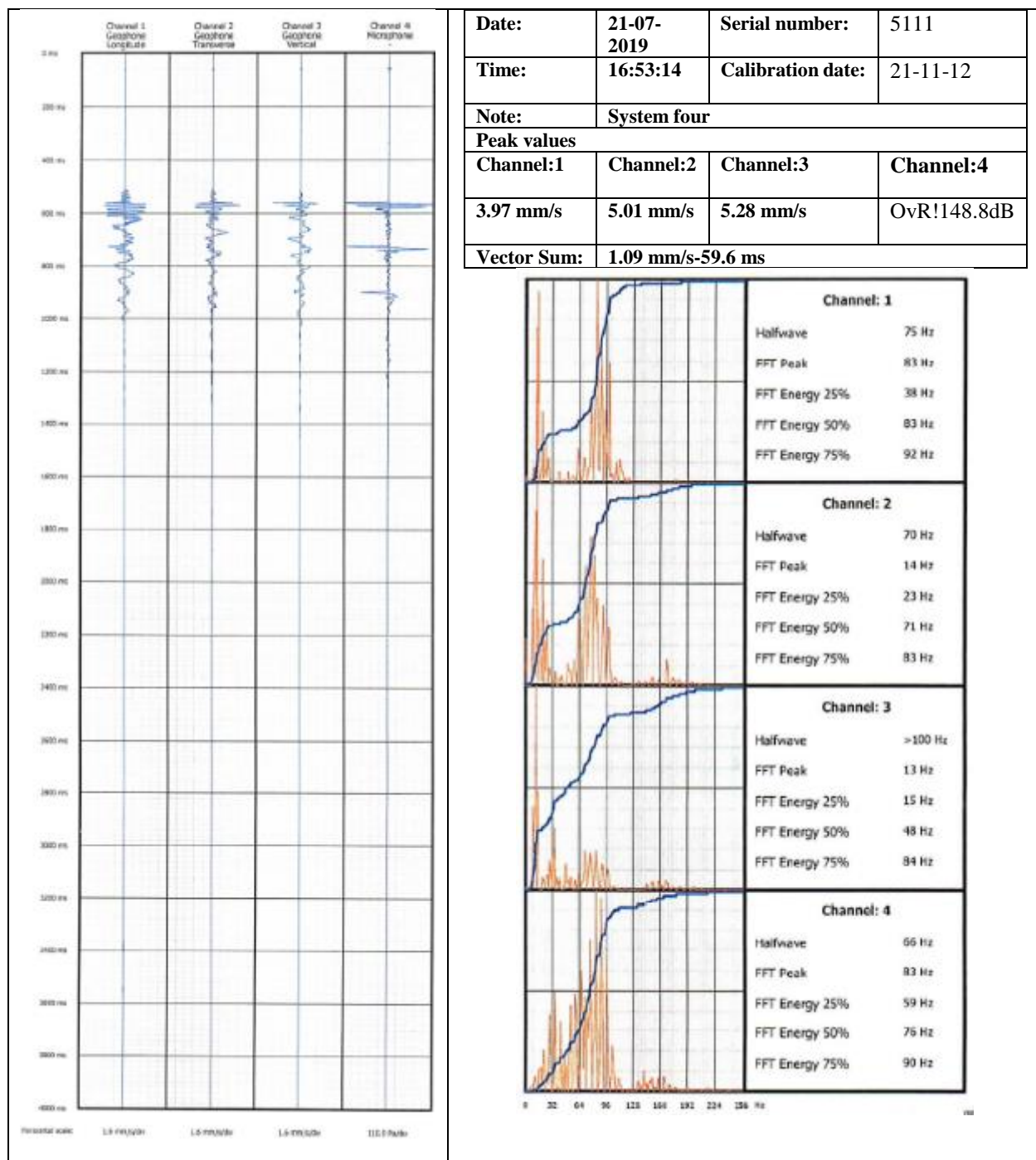


Table 4. Data summary of System 4

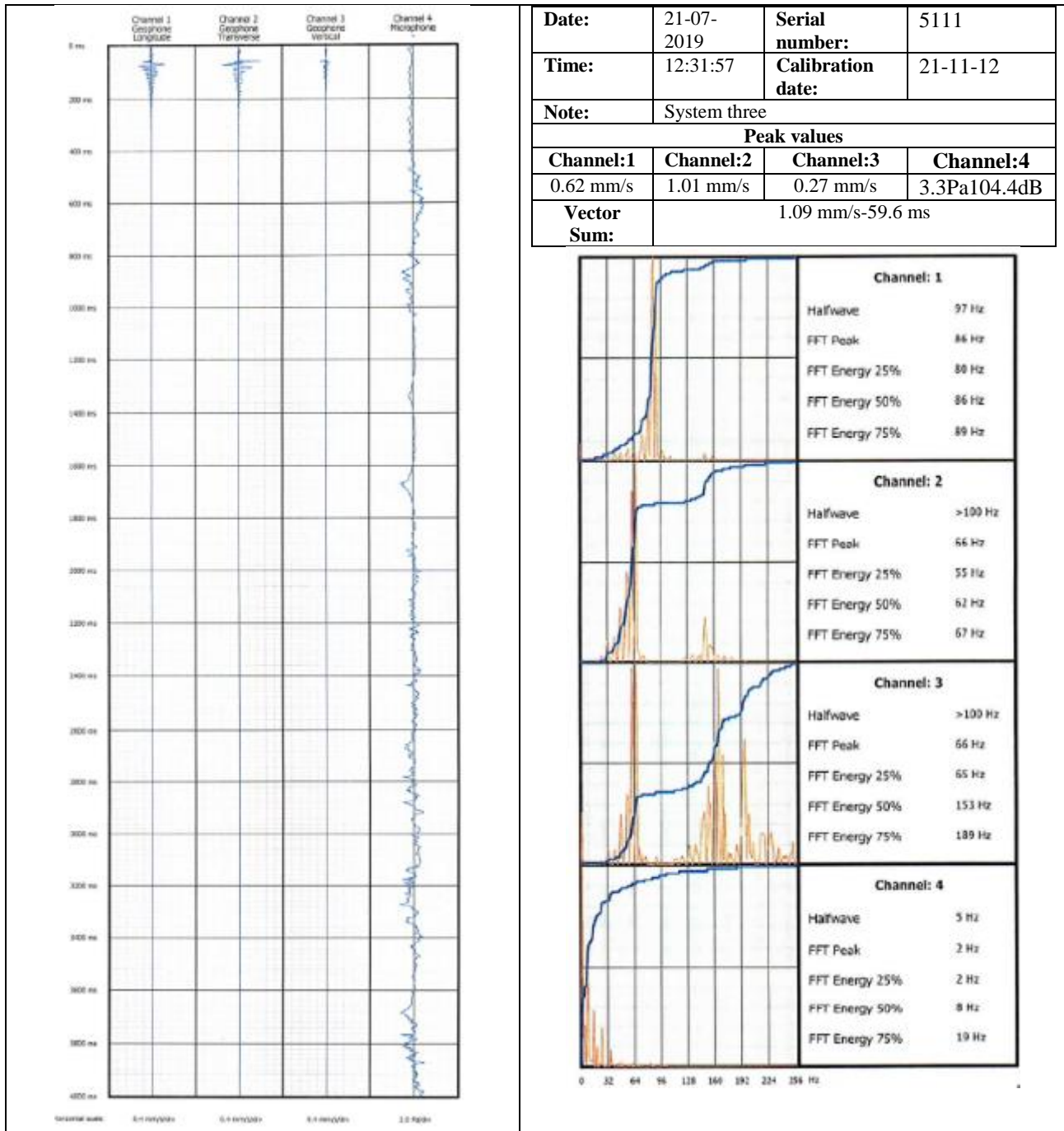


Figure 13. Images of explosions of the third and fourth test setups



Figure 14. Measurements of the crater holes that were formed after the explosions

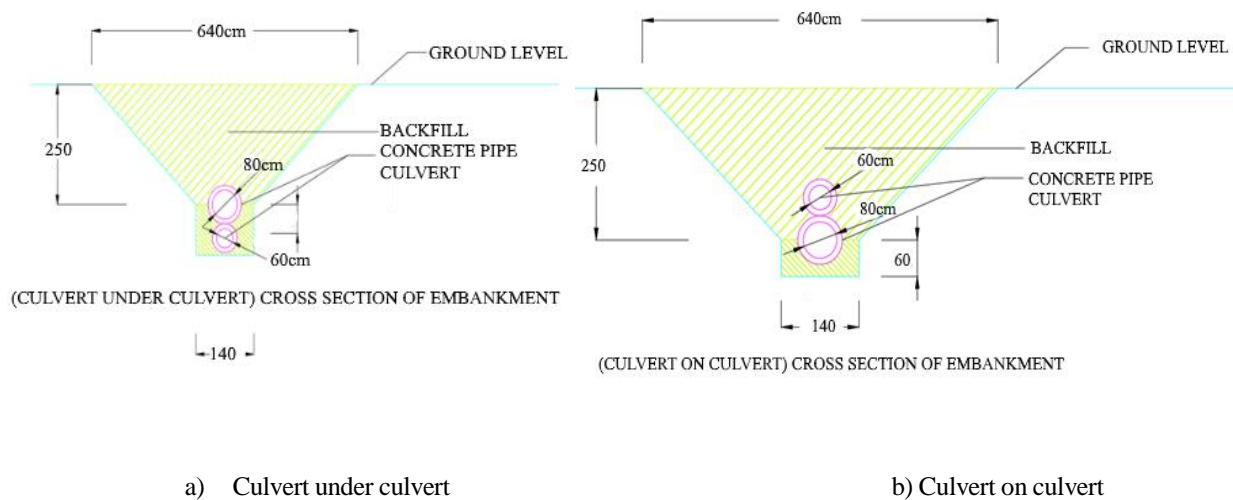


Figure 15. Cross-section of the culvert systems below(a)-above(b) the culvert

4. Conclusion

One of the main methods practiced by terrorist organizations in transportation routes that have sabotage risks is planting explosive materials in culverts that are originally constructed for discharging water. These structures are hard to check visually and they are constructed with thin-walled materials such as concrete culverts. Another goal of choosing concrete culverts is that they are small structures, which enable better compaction and less energy loss in addition to being suitable for lower amounts of explosives. Furthermore, the possibility of planting the explosive setup by a single individual makes these culverts a common choice. When the literature studies are examined;

- Experimentally applied blasting for this type of work is almost nonexistent.
- In the existing studies, experiments were carried out on how many meters deep the pipelines should be placed from the ground.
- As a design, it has been applied as changing the thicknesses and dimensions on type projects.

This study is different from the studies on this subject in the literature. It is thought that it will give important ideas for new designs. In this study, a field study of a full-scale explosion, which was conducted exactly according to terrorist practices, was conducted. The concrete culvert that was analyzed had a diameter of 80 cm. For the explosive material used in the study, 50 kg of ANFO, 1.5 kg of dynamite (3 pieces), and electric detonators were used. For the tests, 3 roads that met the standards were constructed. The practices that were conducted in the study were presented below (Table5).

Table 5. Test setup and the eruptions resulting from explosions

Test Setup	Specification	Aim of Analysis	Explosives	Eruptions
1 st Setup	2.5 m of backfill	impact of explosives	50 kg	430 cm
2 nd Setup	Secondary culvert with 60 cm diameter below primary culvert with 80 cm diameter and 2.5 m of backfill	impact of explosives in the secondary culvert setup below the primary culvert	50 kg	210 cm
3 th Setup	Secondary culvert with 60 cm diameter above primary culvert with 80 cm diameter and 2.5 m of backfill	impact of explosives in the secondary culvert setup above the primary culvert	50 kg	165 cm



Figure 16. Eruptions in the first setup



Figure 17. Eruptions in the third and fourth setups

As a result of the tests in the study, when the results were compared with the typical cross-sections, the largest eruptions were observed in the road with geotextile membrane installation, which was followed by the cross-section of the road with a 60 cm secondary culvert below an 80 cm primary culvert and the road with a 60 cm secondary culvert above an 80 cm primary culvert, respectively (Table 6). In the footage recorded by the stationary cameras, the measurements were conducted by comparing the culverts before and after explosions to designate the eruptions during explosions. When the explosions were ranked according to the crater holes that were created as a result of the explosions, the following rankings were obtained.

Table 6. Crater formation

Measurements of the crater holes that were formed after the explosions				
standard road	50 kg	TNT	150 cm	High Damage
the road with geotextile membrane installation	50 kg	TNT	45 cm	Low Damage
backfill above a culvert with 80 cm diameter	50 kg	TNT	65cm	Low Damage
backfill above a culvert with 60 cm diameter	50 kg	TNT	70 cm	Low Damage
General evolution	50 kg	TNT	60 cm	Low Damage

In these tests, 3 pieces of Riogel Troner (38x3870) cartridge Rionel ms capsules were used in the detonations and the cartridges were measured during the detonations in terms of their VoD values within groups of three in the open. When the cartridges were cut to examine their densities, it was observed that the products were turned into sponge-like structures while maintaining their forms. In the analyses, the VoD value was measure as 3826.70 m/s.

$$\text{Energy of 1 kg of TNT} = 0.238845896627 \times 4.184 \times 10^6 \text{ j} = 1000 \text{ kCal} \quad (1)$$

The relative activity factor of ANFO is 0.42 TNT, which is equal to 420 kCal energy. The amount of ANFO used in the study was 50 kg, which was calculated as the following.

$$50 \times 420 = 21000 \text{ kCal} \quad (2)$$

Here, the VoD value for the ANFO was calculated as 3800 m/s. In theory, 1 kg of TNT produces 70 kPa of pressure within 1 meter. When these values are adapted to ANFO, 30 kPa creates $30 \times 50 = 1500$ kPa of pressure as the totality of the explosive. This equals 150 tons of pressure per square meter. In the current study, when the area of effect was regarded as 20 cm, this value increases logarithmically. However, because the aim of the study was to simulate terrorist activities exactly in the same way, the compaction practices were not conducted extensively. Therefore, certain amounts of energy were still discharged from the sides of the culverts. This caused certain pieces of culverts to hurtle 200-250 meters away from the explosion site. The distances of hurtling were particularly further in the typical cross-sections of the setups with secondary culverts above and below primary culverts.

5. Discussion

For the results of the tests above, two different types of evaluations were conducted. In the first one, the upsurges over culverts during the explosions were evaluated while in the second one, the crater holes that were formed after the explosions were evaluated. According to these evaluations, the installation of secondary culverts below culverts and geotextile membrane installations should be among the typical cross-sections that can be adopted for absorbing explosive energies. Because the tests in the study demanded high financial costs, the number of tests was limited. However, it was believed that the results were sufficient to devise a general idea about the explosion mechanics in question. In typical cross-sections of the setups with secondary culverts below and above primary culverts, the explosive energies were diverted to the sides of the roads rather than over the roads thanks to the secondary culverts. Accordingly, these two techniques can be implemented for the roads to be built in regions that are under terrorist threats.

6. Acknowledgements

This study was conducted with the help of the Firat University Scientific Research Projects Units (FUBAP Project No: MF.18.26), the Malatya Municipality. We are grateful for their financial and technical support.

7. Author Contribution Statement

In this study, Author 1 contributed to the creation of the idea, the design and the literature review, the evaluation of the results obtained, the procurement of the materials used and the analysis of the results; Author 2 contributed to the creation of the idea, spelling, the procurement of the materials used, reviewing the results and checking the paper for content. Author 3 contributed to the creation of the idea, preparation of experimental setups; Author 4 contributed to the checking the article in terms of content and and literature review.

8. Ethics Committee Approval and Conflict of Interest

There is no need for an ethics committee approval in the prepared article. There is no conflict of interest with any person/institution in the prepared article.

9. References

- [1] Almgoy G, Rivkind AI. "Terror in the 21st century: milestones and prospects-part I". *Current Problems in Surgery*, 44(9), 496–554, 2007.
- [2] Khanmohamadi M, Bagheri M, Khademi N, Ghannadpour SF. "A security vulnerability analysis model for dangerous goods transportation by rail-Case study: Chlorine transportation in Texas-Illinois". *Safety Science*, 110, 230–241, 2018
- [3] Elias W, Albert G, Shiftan Y. "Travel behavior in the face of surface transportation terror threats". *Transport Policy*, 28, 114–122, 2013.
- [4] Beveridge A. *Forensic Investigation of Explosions*. second edition. New York, USA, CRC press, 2011.
- [5] Milliyet. "Silvan'da yine faciadan dönüldü".
<https://www.milliyet.com.tr/yerele-haberler/diyarbakir/silvan-da-yine-faciadan-donuldu-11124018>
(21.12.2015).
- [6] Haberler. "Menfez altına yerleştirilmiş 225kilogram Amonyum Nitrat imha edildi".
<https://www.haberler.com/guncel/mardin-de-menfez-altina-yerlestirilmis-225-8465444-haber/> (24.05.2016)
- [7] Vatan. "İşte PKK tünelleri". [https://www.gazetevatan.com/arsiv/galeri-iste-pkk-tunelleri-1525795\(16.01.2017\)](https://www.gazetevatan.com/arsiv/galeri-iste-pkk-tunelleri-1525795(16.01.2017)).
- [8] Habertürk. "Bitlis'te 350 kilogram patlayıcı imha edildi".
[https://www.haberturk.com/yerele-haberler/haber/11768348-bitliste-350-kilogram-patlayici-imha](https://www.haberturk.com/yerele-haberler/haber/11768348-bitliste-350-kilogram-patlayici-imha-edildi) edildi
(29.04.2017).
- [9] Yenişafak." Eruh'ta el yapımı patlayıcı ile saldırısı: 5 korucu yaralı".
[https://www.yenisafak.com/video-galeri/gundem/eruhta-el-yapimi-patlayici-ile-saldirisi-5-korucu-yarali-](https://www.yenisafak.com/video-galeri/gundem/eruhta-el-yapimi-patlayici-ile-saldirisi-5-korucu-yarali-2106952)
2106952 (28.08.2016).
- [10] Kristoffersen M, Hauge K.O, Børvik T. "Blast loading of concrete pipes using C-4 charges". *Multidisciplinary Digital Publishing Institute Proceedings*, 2(8),428,2018.
- [11] Bonalumi P, Colombo M, Prisco MD. "Internal explosions in embedded concrete". *Applied Mechanics and Materials*, 82, 452–457,2011.
- [12] Olarewaju AJ, Rao NSVK, Mannan MA. "Blast effects on underground pipes". *Electronic Journal of Geotechnical Engineering*, 15, 1–14, 2010.
- [13] Olarewaju AJ, Rao NSV, Mannan MA. "Guidelines for the design of buried pipes to resist effects of internal explosion, open trench and underground blasts". *Electronic Journal of Geotechnical Engineering*, 15, 1–13, 2010.
- [14] Parviz M, Aminnejad B, Fiouz A. "Numerical simulation of dynamic response of water in buried pipeline under explosion". *KSCE Journal of Civil Engineering*, 21(7), 2798–2806, 2017.
- [15] Tang Q, Jiang N, Yao Y, Zhou C, Wu T. "Experimental investigation on response characteristics of buried pipelines under surface explosion load". *International Journal of Pressure Vessels and Piping*, 183, 104101,

2020.

- [16] Chen B, Sun L. "The impact of soil properties on the structural integrity of high-fill reinforced concrete culverts". *Computers and Geotechnics*, 52 , 46–53,2013.
- [17] Kolisoja P, Kalliainen A. "Modelling of plastic culvert and road embankment interaction in 3D", *Procedia Engineering*, 143, 427–434, 2016.
- [18] Marr AJ, Groves DM. " Ion mobility spectrometry of peroxide explosives tatp and HMTD". *International Journal for Ion Mobility Spectrometry*, 59–63, 2003.